Journal Pre-proofs

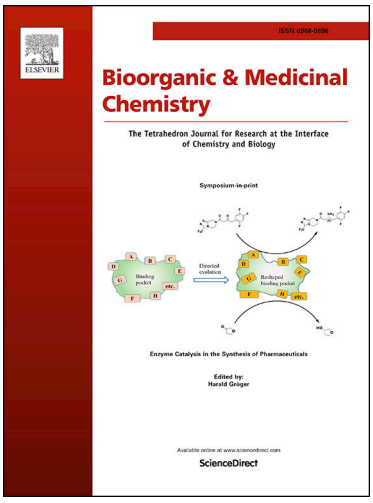

Design, synthesis, and bioactivity of dihydropyrimidine derivatives as kinesin spindle protein inhibitors

Haytham O. Tawfik, Mervat H. El-Hamamsy, Nabaweya A. Sharafeldin, Tarek F. El-Moselhy

PII: S0968-0896(19)31159-9
DOI: https://doi.org/10.1016/j.bmc.2019.115126
Reference: BMC 115126

To appear in: *Bioorganic & Medicinal Chemistry*

Received Date: 9 July 2019
Revised Date: 12 September 2019
Accepted Date: 18 September 2019

Please cite this article as: H.O. Tawfik, M.H. El-Hamamsy, N.A. Sharafeldin, T.F. El-Moselhy, Design, synthesis, and bioactivity of dihydropyrimidine derivatives as kinesin spindle protein inhibitors, *Bioorganic & Medicinal Chemistry* (2019), doi: https://doi.org/10.1016/j.bmc.2019.115126

Design, synthesis, and bioactivity of dihydropyrimidine derivatives as kinesin spindle protein inhibitors

Haytham O. Tawfik, Mervat H. El-Hamamsy, Nabaweya A. Sharafeldin, and Tarek F. El-Moselhy

1. **Haytham O. Tawfik, MSc**
   Assistant Lecturer, Department of Pharmaceutical Chemistry,
   Faculty of Pharmacy, Tanta University, El Giesh street, Tanta, 31527, Egypt.
   Email: haytham.omar.mahmoud@pharm.tanta.edu.eg
   Tel. +201005356819; Fax: +20403335466

2. **Mervat H. El-Hamamsy, PhD**
   Associate Professor, Department of Pharmaceutical Chemistry,
   Faculty of Pharmacy, Tanta University, El Giesh street, Tanta, 31527, Egypt.
   Email: mhamamsy@pharm.tanta.edu.eg
   Tel. +201008121831

3. **Nabaweya A. Sharafeldin, PhD**
Associate Professor, Department of Pharmaceutical Chemistry,
   Faculty of Pharmacy, Tanta University, El Giesh street, Tanta, 31527, Egypt.
   Email: nabawia.eldeen@pharm.tanta.edu.eg
Tel. +201022489700

4. **Tarek F. El-Moselhy, PhD**
   Professor and Chairman of the Department of Pharmaceutical Chemistry,
   Faculty of Pharmacy, Tanta University, El Giesh street, Tanta, 31527, Egypt.
   Email: tarek.faathy@pharm.tanta.edu.eg
   Tel. + 201006358839

Design, synthesis, and bioactivity of dihydropyrimidine derivatives as kinesin spindle protein inhibitors

Haytham O. Tawfik*, Mervat H. El-Hamamsy, Nabaweya A. Sharafeldin and Tarek F. El-Moselhy

Department of Pharmaceutical Chemistry, Faculty of Pharmacy, Tanta University, Tanta, 31527, Egypt.

*Corresponding author: H. O. Tawfik, E-mail: haytham.omar.mahmoud@pharm.tanta.edu.eg
Tel: +201005356819; Fax: +2040-3335466

Abstract

A series of twenty-one 3,4-dihydropyrimidine derivatives bearing the heterocyclic 1,3-benzodioxole at position 4 in addition to different substituents at positions 2, 3 and 5 were designed and synthesized as monastrol analogs. The novel synthesized compounds were screened for their cytotoxic activity towards 60 cancer cell lines according to NCI (USA) protocol. Compounds **10b** and **15** showed the best antitumor activity against most cell lines. Compound **15** was subsequently tested in 5-doses mode and displayed high selectivity towards CNS, prostate and leukemia subpanel with selectivity ratios of 22.30, 15.38 and 12.56, respectively at GI_{50} level. The IC_{50} of compounds **9d**, **10b**, **12, 15** and **16** against kinesin enzyme were 3.86 ± 0.12, 10.70 ± 0.35, 3.95 ± 0.12, 4.36 ± 0.14, and 14.07 ± 0.45 μM respectively, while the prototype compound, monastrol, reported IC_{50} value of 20 ± 0.42 μM. The safest compound among test compounds against normal cell line (HEK 293) is **10b** with IC_{50} value of 62.02 ± 2.42 μM/ml in comparison to doxorubicin (IC_{50} = 11.34 ± 0.44 μM/ml). Cell cycle analysis of SNB-75 cells treated with compound **15** showed cell cycle arrest at G2/M phase. Further, the assay of levels of active caspase-3 and caspase-9 was investigated. Moreover, Molecular docking of compounds, **9d**, **10b**, **12**, **15**, **16**, monastrol and mon-97 was performed to study the interaction between inhibitors and the kinesin spindle protein allosteric binding site.

Keywords: Dihydropyrimidine; kinesin spindle protein; cell cycle analysis; apoptosis; molecular docking.

1. Introduction

Kinesins are class of motor proteins that responsible for many central purposes inside the cell [1, 2]. Generally, these proteins bind to microtubules and use the energy resulting from ATP hydrolysis to complete their roles. The mitotic kinesin, a subclass of kinesin, is expressed in cell division at mitotic phase to establish the mitotic spindle, and other roles [3]. One of the features of cancer cells is uncontrolled cell proliferation. The classical chemotherapeutic drug like taxanes (paclitaxel) and Vinca alkaloids (vincristine, vinblastine), that interfering with microtubule dynamics, are still as anticancer agents used in the clinic [4, 5]. However, due to the presence of microtubules in non-dividing cells such as, post-mitotic neurons, unwanted side effects, like peripheral neuropathy, are

often detected in patients treated with these drugs [6]. The mitotic kinesin family consists of more than 10 members, which show either unique or overlapping roles in mitosis [7]. Kinesin spindle protein (KSP, or Eg5), is considered the most dramatic target protein of the mitotic kinesin family. KSP contains a catalytic ATPase activity that provides energy for directed movement along microtubules. Therefore, inhibition of ATPase activity will trouble the role of KSP effectively. Most of KSP inhibitors are ATP-uncompetitive allosteric inhibitors that inhibit ATPase activity reversibly and include diverse of structural categories. Recently, many KSP inhibitors have entered pre-clinical and clinical trials as anticancer agents and have revealed satisfying effect with IC_{50} of sub-nanomolar to low nanomolar levels [8]. From monastrol having dihydropyrimidine nucleus, the earliest found KSP inhibitor but did not enter clinical trial, passing by s-trityl-l-cysteine (STLC), dihydropyrroles and dihydropyrazoles (e.g. MK-0731, Arry-520), which have entered phase I and II clinical trials, to quinazolines (e.g. ispinesib) which has entered a phase II clinical trial, KSP is still promising target for designing new anticancer agents [9].

In 1999, Mayer et al, discovered monastrol (**Figure 1**) as the first small molecule able to inhibit several targets as anticancer including; the mitotic kinesin Eg5 (KSP) [10-12], 5-lipoxygenase enzyme [13], mTOR [14], and cell division cycle 25 (CDC25) phosphatases [15]. Monastrol causes mitotic arrest at G2/M phase by blocking bipolar mitotic spindle in mammalian cells leading to cell apoptosis [16, 17]. Monastrol has motivated the medicinal chemists to utilize structure-based drug design methods to design new antimitotic agents through structural manipulation of the dihydropyrimidine (DHPM) scaffolds to generate novel compounds for cancer therapy. [9, 18]

2. Rationale and Design

Dihydropyrimidine (DHPM) derivatives were synthesized by Biginelli [19] through multi-component reaction. Many DHPM-based derivatives have presented important biological functions including antitumor and other biological activities [20]. Since the discovery of monastrol (IC_{50} = 20 ± 0.42 μM) (**Figure 1A**) as a weak antimitotic anticancer DHPM derivative, many attempts have been reported to develop more potent inhibitors of kinesin Eg5 based on monastrol scaffold [21-23]. Piperastrol (**Figure 1A**), the 3,4-methylenedioxy analogue of monastrol, (IC_{50} = 6.6 μM) was found to be more effective than monastrol against OVCAR03 cancer cell line [12, 24, 25]. The presence of benzyl ester at position 5 of DHPM [26] enhanced the anticancer activity as shown in compound **1**, (IC_{50} = 55 ± 3.37 μM) against MCF7 and HeLa (IC_{50} = 40 ± 2.43 μM) cancer cell lines [27], (Figure 1B). Moreover, replacement of ester with ketone analogues at 5 position resulted in a more potent inhibitor, mon-97 (IC_{50} = 0.1 ± 0.02 μM) [23] (**Figure 1C**). In addition, cyclic ketone analogues conferred rigidity to the conformation of DHPM, as presented in dimethylenastron (IC_{50} = 0.2 ± 0.11 μM), (**Figure 1C**) and improved the potency 100-time relative to monastrol [28]. Furthermore,

compound **2**, the hybrid of DHPM and benzimidazole ring, (**Figure 1D**) exhibited anticancer activity against PC3 (IC_{50} = 37 µM) and NCIH1299 (IC_{50} = 40 µM) cancer cell lines [29].

Motivated by the aforementioned findings, we have utilized rational chemical approaches to design and synthesize novel DHPM derivatives as potential kinesin inhibitors for cancer therapy. In this study, the integration of the benzyl ester moiety into the piperastrol skeleton afforded analogues **8a-h** which upon acylation of 3-NH of DHPM ring resulted in analogues **9a-d** as shown in (**Figure 1E**). However, incorporation of different ketone or cyclic ketone moieties into piperastrol skeleton yielded analogues **10**, **11** and **12** (**Figure 1F**). Moreover, we designed the new analogue, **15**, (**Figure 1G**) as a result of the amalgamation between active moieties; benzyl ester, benzimidazole with piperastrol nucleus. Lastly, we designed the new analogue, **16**, (**Figure 1H**) as a hybrid of ketone side chain, heterocyclic benzimidazole and piperastrol.

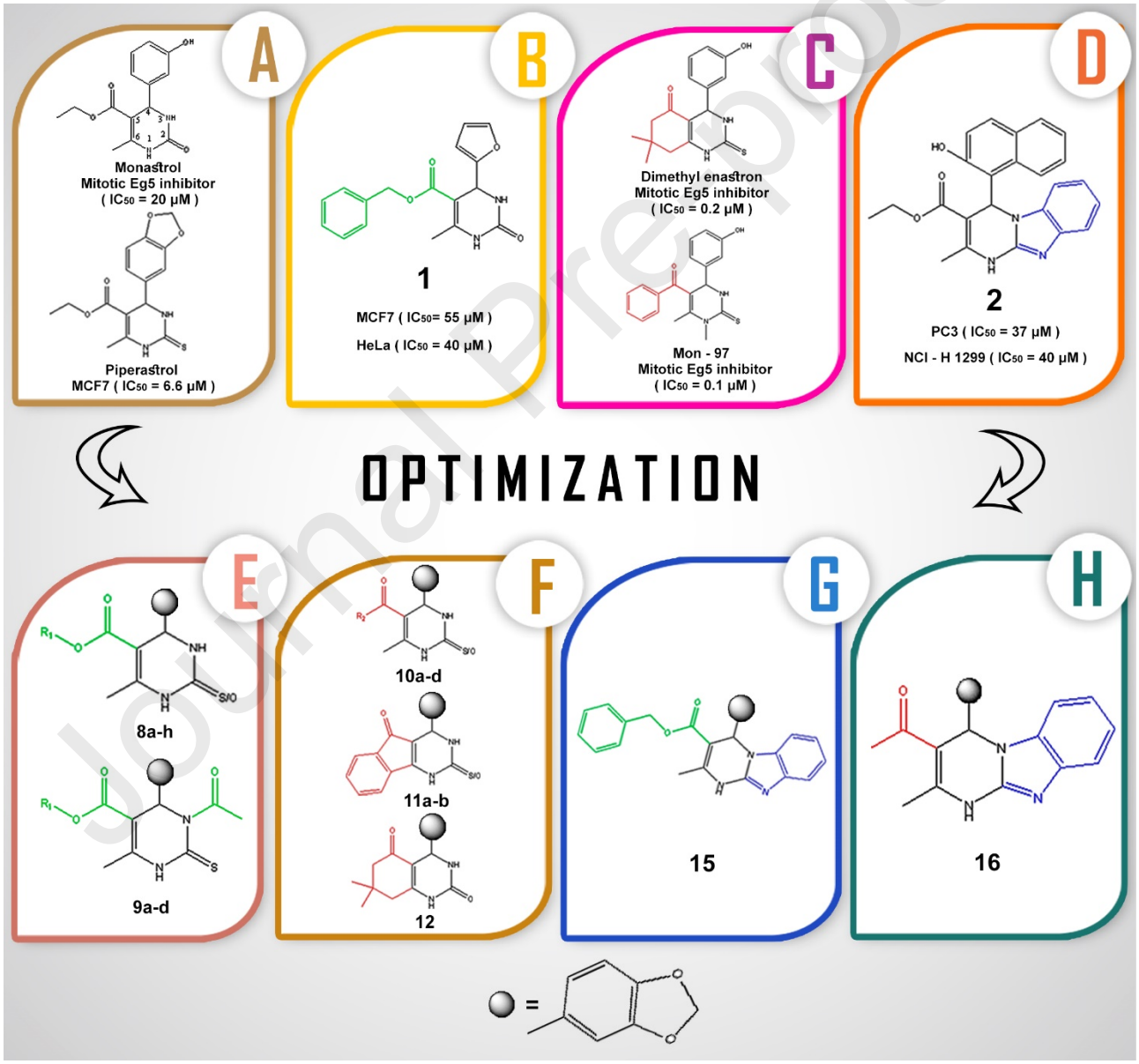

Figure 1. The workflow of the rational structure-based design strategy in this study

3. Results and Discussion

3.1. Chemistry

As shown in **Scheme 1**, Williamson method was employed through the nucleophilic substitution reaction between 3,4-dihydroxybenzaldehyde **3** and dichloromethane under basic condition to afford, 1,3-benzodioxole-5-carbaldehyde (piperonal) [30, 31].

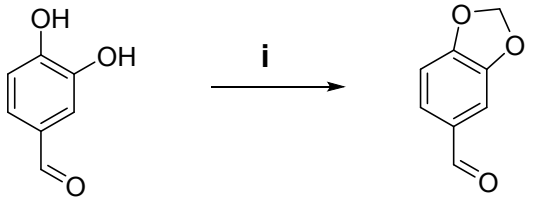

Scheme 1. Synthesis of 1,3-benzodioxole-5-carbaldehyde **4**. Reagents and conditions: (i) CH_2Cl_2, K_2CO_3, DMF, reflux, 12 h.

Different acetoacetate derivatives were prepared according to the modified Clemens method via condensation of 2,2,6-trimethyl-1,3-dioxin-4-one (TMD) with different alcohols (5a-d) in refluxing xylene [32-34] **(Scheme 2)**.

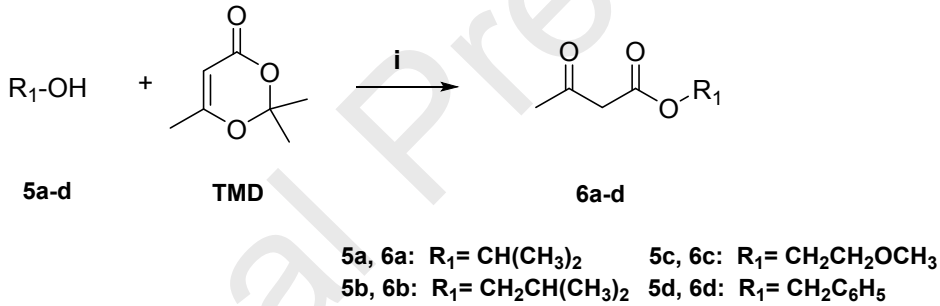

Scheme 2. Synthesis of acetoacetate derivatives **6a-d**. Reagents and conditions: (i) TMD, xylene, reflux, 6 h.

As presented in **Schemes 3** and **4**, racemic mixture of DHPM derivatives, **8a-h**, **10a-d**, **11a-b** and **12,** were conveniently prepared via multicomponent reaction, of Biginelli type [35]. Under acidic condition, cyclocondensation of 1,3-benzodioxole-5-carbaldehyde **4**, thiourea **7a** or urea **7b** and active methylene compounds such as acetoacetates **(6a-d)** or β-diketones afforded racemic mixture of target compounds **8a-h**. 3-N-acetyl DHPM derivatives **9a-d** in **Scheme 3** were prepared by heating DHPM derivatives (**8a-d**) with acetic anhydride for 5h [36]. In case of compound **12**, it was previously synthesized by microwave irradiation technique [37].

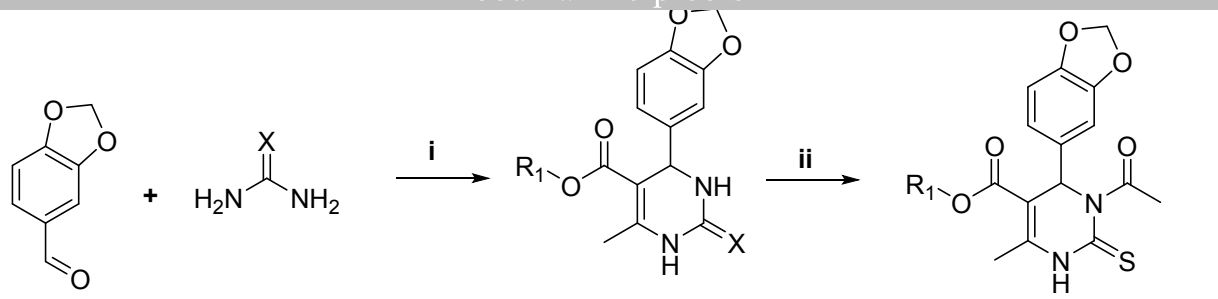

4 **7a-b** **8a-h** **9a-d**

7a: X=S
7b: X=O

8a: X=S, R_1= $CH(CH_3)_2$
8b: X=S, R_1= $CH_2CH(CH_3)_2$
8c: X=S, R_1= $CH_2CH_2OCH_3$
8d: X=S, R_1= $CH_2C_6H_5$
8e: X=O, R_1= $CH(CH_3)_2$
8f: X=O, R_1= $CH_2CH(CH_3)_2$
8g: X=O, R_1= $CH_2CH_2OCH_3$
8h: X=O, R_1= $CH_2C_6H_5$

9a: R_1= $CH(CH_3)_2$
9b: R_1= $CH_2CH(CH_3)_2$
9c: R_1= $CH_2CH_2OCH_3$
9d: R_1= $CH_2C_6H_5$

Scheme 3. Synthesis of DHPM derivatives **8a-h** and acetylated DHPM derivatives **9a-d**. Reagents and conditions: (i) Different acetoacetates **(6a-d)**, citric acid, TEOF, reflux, 10 h; (ii) Acetic anhydride, reflux, 5 h.

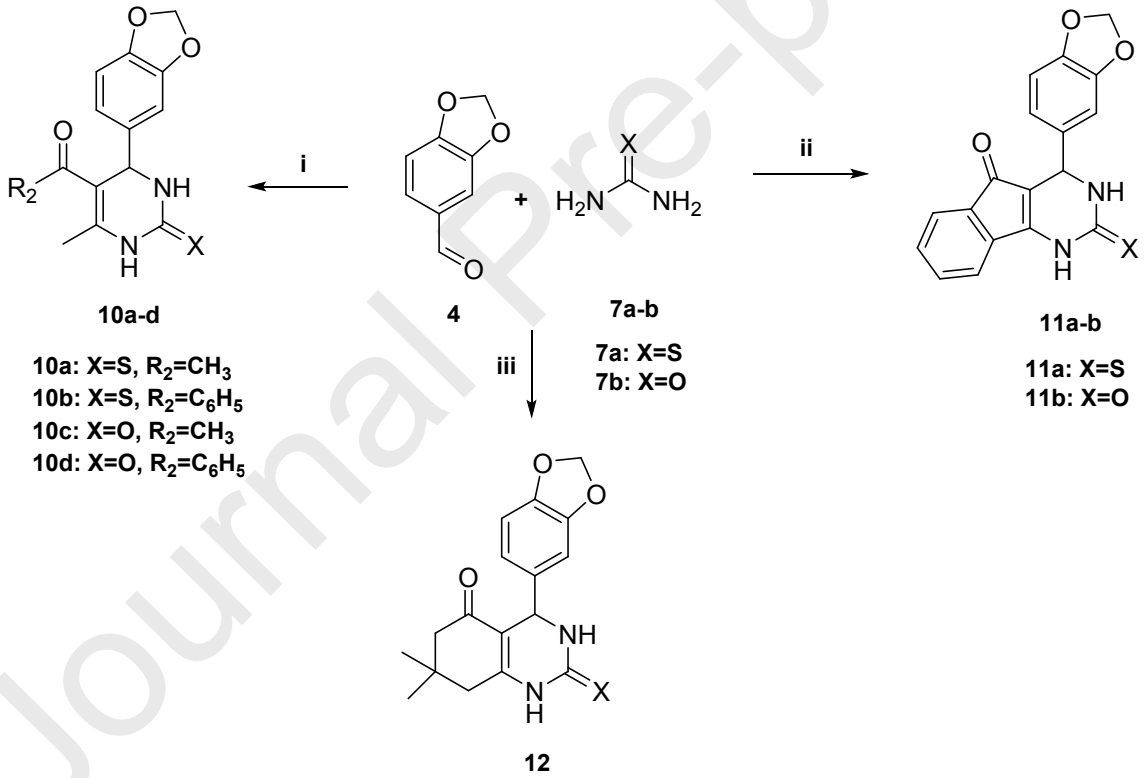

10a-d **4** **7a-b** **11a-b** **12**

10a: X=S, R_2=CH_3
10b: X=S, R_2=C_6H_5
10c: X=O, R_2=CH_3
10d: X=O, R_2=C_6H_5

7a: X=S
7b: X=O

11a: X=S
11b: X=O

Scheme 4. Synthesis of monocyclic DHPM derivatives, **10a-d**, tricyclic DHPM derivatives, **11a-b,** and bicyclic DHPM derivative, **12**. Reagents and conditions: (i) Different β-diketones, citric acid, TEOF, reflux, 10 h; (ii) 1,3-indandione, citric acid, TEOF, reflux, 10 h; (iii) Dimedone, citric acid, TEOF, reflux, 10 h.

2-Aminobenzimidazole **14** was synthesized by reacting 1,2-phenylenediamine **13** with cyanogen bromide, followed by neutralization with concentrated ammonium hydroxide [38] as shown in **Scheme 5**.

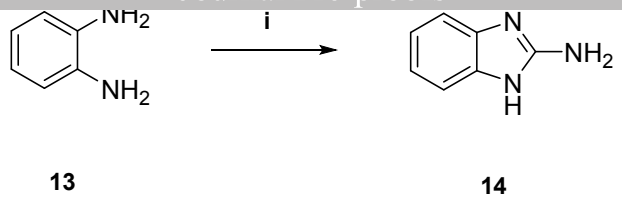

13 14

Scheme 5. Synthesis of 2-aminobenzimidazole **14**. Reagents and conditions: (i) CNBr, ethanol/water, DMF, reflux, 1 h.

As reported in **Scheme 6**, one-pot cyclocondensation of 1,3-benzodioxole-5-carbaldehyde **4**, 2-aminobenzimidazole **14** with acetyl acetone or benzyl acetoacetate carried out in DMF afforded the novel tricyclic DHPM derivatives, **15** and **16**, respectively [29].

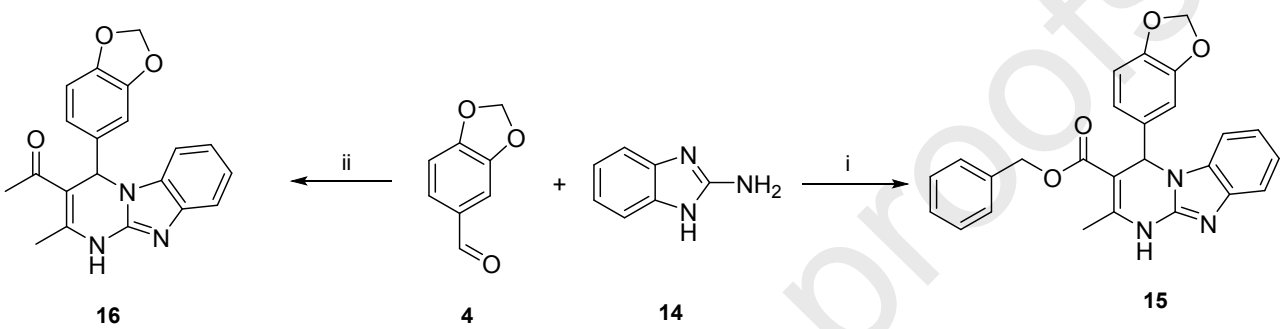

16 4 14 15

Scheme 6. Synthesis of hybrid DHPM derivatives **15** and **16**. Reagents and conditions: (i) Benzyl acetoacetate, DMF, reflux, 10 h; (ii) Acetyl acetone, DMF, reflux, 10 h.

Elemental analysis and the spectroscopic data (^{1}H NMR, ^{13}C NMR, and mass spectroscopy) of the synthesized compounds are in concord with the expected chemical structures as given in the experimental section later.

The ^{1}H NMR spectrum of compound **11b**, as a representative example, was characterized by a singlet signal at δ = 6.22 ppm of the two protons of dioxolane ring. A doublet signal at 7.14 ppm was observed for the 6-H of the benzodioxole moiety. The 4-H proton of the dihydropyrimidine moiety resonated at 7.78 ppm as a singlet. Besides, multiplet signals at 7.93 – 8.01 ppm with seven protons integration, were assigned for; four protons at 6,7,8,9-H_4 of indene moiety, one proton at 6-H of benzodioxole moiety and two protons at 1,3-H_2 of the dihydropyrimidine part. Moreover, a doublet signal at 8.53 ppm is assigned for the 4-H of benzodioxole which showed meta-coupling to the 6-H of benzodioxole moiety. Further, ^{1}H-^{1}H COSY spectrum of compound **11b** supported this assignment (See Supplementary Data).

^{13}C NMR spectral assignment of all the synthesized compounds has been made. ^{13}C NMR (on-resonance & DEPT) spectra of compound **11b** showed the signals resonated at: 102.94, 109.30, 112.32, 133.63, 139.75, and 148.23 ppm are assigned to seven carbons of benzodioxole moiety, while the signals resonated at: 123.36, 123.47, 128.03, 136.15, 136.27, and 142.24 ppm are assigned to six carbons of benzene ring of indene moiety. The three signals for the dihydropyrimidine core at 127.06 ppm for C-5, 146.42 ppm for C-4, and 152.79 ppm for C-6 were observed. The signals resonated in

the deshielded region at 189.53, and 190.20 ppm are assigned to two C=O carbons. Moreover, ^{1}H-^{13}C Heteronuclear single quantum coherence (HSQC) spectrum of compound **11b** supported this assignment and added strong evidence for this elucidation (See supplementary material).

3.2. Biological evaluation

3.2.1. In vitro anticancer screening at NCI-USA

The novel twenty-one synthesized compounds were acquiesced to the National Cancer Institute "NCI" (www.dtp.nci.nih.gov), Bethesda, Maryland, USA. All submitted compounds were nominated on the basis of the degree of structural diversity and computer modelling techniques for the evaluation of their antineoplastic activity. The screening of activity passes through two possible processes, commencing with the assessment of all compounds against 60 cell lines on nine types of human tumor at a single dose of 10 μM. The output from the single dose screening is covered as a mean graph, and it became available to be analyzed by the COMPARE program. Finally, the compounds which exhibit significant growth inhibition get to pass the assessment against the 60 cell lines at five doses including the one mentioned before.

3.2.1.1. In vitro single-dose (10 μM) anticancer screening on NCI 60 cell panels

The synthesized target compounds (**8a-h**, **9a-d**, **10a-d**, **11a-b**, **12**, **15** and **16**) were initially subjected to *in vitro* one dose anticancer assay in full NCI 60 cell lines panel represented by nine human systems, including, Leukemia (L), Non-Small Cell Lung Cancer (NSCLC), Colon Cancer (CC), Central Nervous System Cancer (CNSC), Melanoma (M), Ovarian Cancer (OC), Renal Cancer (RC), Prostate Cancer (PC), and Breast Cancer (BC) in agreement with the protocol of the NCI, USA. The compounds were added at 10 μM and the culture was incubated for 48h. Endpoint determinations were carried out with a protein binding dye, sulforhodamine B. Later, the outcomes of all tested compounds were described as a percentage growth of the treated cells compared to the unprocessed control cells. The mean-graph midpoint values (MG-MID) are described in **Table 1**.

Table 1. The mean-graph midpoint (MG-MID) values of percentage growth of all tested compounds

Cpd. no.	NSC code	L	NSCLC	CC	CNSC	M	OC	RC	PC	BC	MG-MID
8a	808610	102.89	100.16	107.45	98.35	98.85	104.61	99.82	97.45	99.90	101.26
8b	808612	95.02	103.61	108.14	101.02	102.49	102.95	100.90	96.92	98.31	101.66
8c	800517	97.58	100.58	104.94	101.26	101.62	105.19	100.78	101.86	100.51	101.64
8d	**800516**	**77.29**	**96.37**	**102.40**	**99.49**	**98.72**	**98.81**	**93.01**	**92.88**	**91.79**	**95.07**
8e	808609	109.55	104.95	107.64	101.09	102.37	104.47	99.01	104.31	100.29	103.62
8f	808611	105.04	103.86	107.71	101.92	103.18	105.11	101.96	100.47	103.78	103.90
8g	809235	100.37	101.73	101.94	96.76	101.96	101.45	96.31	103.24	101.51	100.43
8h	**808618**	**100.73**	**100.59**	**105.83**	**97.42**	**98.69**	**102.39**	**97.53**	**95.96**	**94.09**	**99.61**
9a	**810528**	**87.12**	**94.22**	**101.34**	**97.61**	**101.81**	**103.66**	**102.09**	**95.49**	**92.89**	**97.88**
9b	**810529**	**81.34**	**93.53**	**98.97**	**96.61**	**98.96**	**97.35**	**98.58**	**90.38**	**88.19**	**94.77**
9c	**810531**	**98.27**	**95.41**	**103.16**	**95.30**	**99.64**	**98.98**	**97.97**	**101.87**	**98.12**	**98.47**
9d	**810530**	**50.65**	**87.32**	**73.71**	**80.12**	**79.46**	**94.70**	**89.76**	**88.17**	**79.84**	**81.67**

10a	809237	100.63	103.27	107.04	98.38	104.37	104.68	99.64	104.45	104.22	102.94
10b	**812017**	**25.88**	**54.06**	**32.33**	**43.89**	**38.25**	**50.76**	**45.01**	**70.10**	**49.55**	**43.81**
10c	809236	102.41	102.04	106.20	100.58	104.52	105.90	100.96	108.33	103.12	103.41
10d	813491	100.21	99.60	103.93	98.40	99.15	101.89	97.70	104.00	99.53	100.17
11a	809243	104.17	100.91	106.60	96.35	105.86	104.74	99.05	104.30	100.99	102.51
11b	809242	104.49	101.95	108.00	95.22	104.72	108.00	99.23	107.52	102.66	103.25
12	**808614**	**106.67**	**108.59**	**109.68**	**104.30**	**103.48**	**106.17**	**105.81**	**103.14**	**109.14**	**106.55**
15	**812015**	**18.45**	**46.87**	**27.44**	**26.86**	**34.31**	**43.32**	**59.12**	**47.31**	**32.86**	**35.21**
16	**810527**	**91.39**	**98.38**	**103.96**	**98.66**	**104.73**	**104.76**	**101.65**	**101.14**	**97.72**	**100.52**

Compounds showed strong (**10b** and **15**) and low (**8d**, **8h, 9a-d 12** and **16**) cytotoxic activity selected for the next step, one dose full panel analysis, are in bold.

Data analysis of the mean-graph midpoint (MG-MID) values revealed that, compounds **10b** and **15** showed the most potent cytotoxicity with MG-MID values of 43.81% and 35.21% respectively. Moreover, they showed broad spectrum activity against all tested cancer cell lines while, remain compounds showed mild cytotoxic activity as indicated in **Table 1**.

Consequently, out of the screened twenty-one target compounds, ten hybrids composed of strong (**10b** and **15**) and low (**8d**, **8h**, **9a-d 12** and **16**) cytotoxic compounds were successfully taken to the next step, one dose full panel analysis for evaluation of cytotoxic activity against NCI 60 human tumor cell lines. The percentage of cell growth are presented in **Table S1** (supplementary material).

Since the result reported for the single dose assay was growth percentage of the treated cells, this allows detection of both growth inhibition (when subtract growth percentage from 100, values from 0 to 100) and lethality (values less than zero). For example, a growth percentage value of 100 means zero growth inhibition. A growth percentage value of 60 would mean 40% growth inhibition. A growth percentage value of zero means no net growth by the treatment. A growth percentage value of -60 would mean 60% lethality. A value of -100 means all cells are dead [39].

As given in **Table S1**, compound **15** (NSC 812015) demonstrated the most remarkable and potent cytotoxic activity against the different NCI cell panel. Regarding lethality, compound **15** displayed lethal effect against leukemia, cancer HL-60 (TB) by (-14.74 %), CNS cancer SNB-75 by (-6.67 %), melanoma MDA-MB-435 by (-35.36 %), and renal A498 cancer cell line (-10.15 %) at a single dose assay concentration of 10^{-5} M. Furthermore, compound **10b** revealed the lethal influence on CNS cancer SNB-75 by (-1.40 %), melanoma MDA-MB-435 by (-49.49 %), and renal A498 cancer cell line by (-12.48 %) at a single dose assay.

Data analysis of growth inhibition assay disclosed also that, compound **15** showed a discernible potent activity against a wide variety of different cancer cell lines under investigation. As designated in **Table S1**, Compound **15** displayed growth percentage less than 40 in all leukemia cell lines, NSCLC; NCI-H460 and NCI-H522 cell lines, all colon cancer cell lines (except HCC-2998), all CNSC cell lines (except SF-268 and SNB-19), Melanoma; LOX IMVI, MALME-3M, M14 and SK-MEL-5 cell lines, ovarian cancer; OVCAR-3 and NCI/ADR-RES cell lines, renal cancer; ACHN and

CAKI-1 cell lines, breast cancer; MCF7, HS 578T and MDA-MB-468 cell lines. In addition, compound **10b** exhibited a potent activity against all leukemia cell lines (except CCRF-CEM and RPMI-8226), NSCLC; NCI-H460 and NCI-H522 cell lines, all colon cancer cell lines (except COLO 205 and HCC-2998), CNSC; SF-539 and U251 cell lines, Melanoma; LOX IMVI, M14 and SK-MEL-5 cell lines, ovarian cancer; OVCAR-3 cell line, renal cancer; CAKI-1 cell line, breast cancer; MCF7 and HS 578T cell lines with growth percentage less than 40. Curiously, compound **9d** showed potent and selective cytotoxic activity against leukemia, cancer HL-60 (TB) cell line.

Compounds displayed growth percentage in the range of 60-80 are considered moderately active cytotoxic agents. Data showed that, compound **15** showed moderate activity on the remaining of the cancer cell lines. Moreover, Compound **10b** showed moderate activity on leukemia; CCRF-CEM and RPMI-8226 cell lines, NSCLC; A549, EKVX, HOP-92, NCI-H226, NCI-H23 and NCI-H322M, colon cancer; COLO 205 and HCC-2998, cell lines, CNSC; SF-268, SF-295 and SNB-75, cell lines, Melanoma; MALME-3M, SK-MEL-2, SK-MEL-28, UACC-257 and UACC-62, cell lines, ovarian cancer; IGROV1, OVCAR-5, OVCAR-8, NCI/ADR-RES and SK-OV-3, cell line, all renal cancer (except A498 and CAKI-1), all prostate cancer cell lines, all breast cancer (except MCF7 and HS 578T). Unfortunately, the activity of the other target compounds was in range of moderate (G%, 40-80) and mild (G%, more than 80) depending on their growth percentage values.

3.2.1.1.1. Structure activity relationship

The rationale behind preparing a series of DHPM scaffold bearing different functionalities was to establish a definite structure activity relationship pattern and emphasize the role of structure manipulations in imparting bioactivity. Scanning **Table 1**, we have deduced that, the introduction of sulfur atom into the 2-position of DHPM ring significantly influenced the antitumor activity. For example, compounds **8d** and **10b (**MG-MID, 95.07 and 43.81 respectively) exhibited higher activity than their oxo-analogues **8h** and **10d (**MG-MID, 99.61 and 100.17 respectively). On the other hand, the introduction of acetyl group at the 3-position enhanced the anticancer activity as noticed in compounds **9a-d** with MG-MID values ranged from 97.80 to 81.67 when compared with their non-acetylated analogues **8a-d** with MG-MID values ranged from 101.60 to 95.07. Moreover, the incorporation of a phenyl or benzyl group through a ketone or ester bridge to 5-position of the DHPM ring resulted in significant enhancement of potency as reported in **Table 1** for compounds **10b** and **15** with MG-MID = 43.81 and 35.21 respectively. The presence of alkyl ester in compounds **8a-c (**MG-MID values ranged from 101.26 to 101.66) or alkyl ketone in analogues **10a, c, d** (MG-MID values ranged from 100.17 to 103.41) at 5-position of the DHPM ring revealed lower anticancer activity. The inclusion of the carbonyl group at the 5-position into a cyclic structure either in a cyclohexanone as observed in **compound 12** (MG-MID = 106.55) or indenone ring in compounds

11a-b (MG-MID = 102.51 and 106.25 respectively) diminished the cytotoxic activity. Compound **15** (MG-MID = 35.22) having benzimidazole moiety and benzyl ester group has emerged as the most promising antimitotic anticancer compound of this series while its methyl ketone analogue, compound **16** demonstrated much lower potency with MG-MID value of 100.51. Accordingly, substituents at different positions of the DHPM ring played an important role in controlling the anticancer activity of our target compounds. Free nitrogen at position-1 as well as sulfur atom at position-2 were favored, while free nitrogen at position-3 was not essential for activity. Finally, lipophilic groups, such as phenyl and benzyl, at position-5 were markedly enhanced the activity. The aforementioned SAR was supported by the docking study on later section.

3.2.1.2. In-vitro 5 doses full NCI 60 cell panel assay

The tested compounds which satisfied scheduled threshold growth inhibition criteria would further be selected for NCI full panel five dose assay at tenfold dilutions of five concentrations (0.01, 0.1, 1, 10 & 100 μM) ranging from 10^{-4} to 10^{-8} M against all the NCI 60 tested cell lines. Accordingly, compound **15** (NSC 812015), which fulfilled predetermined threshold inhibition criteria, was selected for additional screening at 5-log dose molar range. The consequences, of cytotoxic activity of compound **15**, were used to create log concentration versus % growth inhibition curves and accordingly, three response parameters (GI_{50}, TGI & LC_{50}) were computed for each cell line as listed in **Table S2**. The GI_{50} value (growth inhibitory activity) relates to the concentration of the compound initiating 50% decrease in the net cell growth while, the TGI value (cytostatic activity) is the concentration of the compound resulting in total growth inhibition, and LC_{50} value (cytotoxic activity) is the concentration of the certain compound causing net 50% loss of initial cells at termination of the incubation period of 48 h [39].

It can be deduced from **Table S2** that compound **15** (NSC 812015) exhibited remarkable anticancer activity against most of the tested cell lines representing nine different subpanels at GI_{50} level beginning from 0.08 μM. Analysis of data in **Table S2** revealed that, compound **15** exhibited the highest activity against MDA-MB-435 (Melanoma) with GI_{50} of 0.08 μM and least activity against NCI-H226 (Non-Small Cell Lung Cancer), SK-MEL-28 (Melanoma), OVCAR-5 (ovarian cancer) and TK-10 (Renal Cancer) with GI_{50} > 100 μM. The best value of TGI was noted on MDA-MB-435 (Melanoma) with 0.35 μM. Toxicity is measured in terms of lethality; compound **15** was not lethal and safe in nature as it is obvious by examining the LC_{50} value >100 μM [40].

The criterion for selectivity of a compound depends upon its selective index, which was obtained by dividing the full panel MIDa (the average sensitivity of all cell lines towards the test agent) by their individual subpanel MIDb (the average sensitivity of all cell lines of a specific subpanel towards the test agent). The ratios between 3 - 6 indicate moderate selectivity, ratios greater than 6 refer to high

selectivity to the corresponding cell line and compounds with ratios less than 3 will be non-selective towards the corresponding subpanel. Compound **15** exhibited selectivity ratios ranging from 0.46 to 22.30 at the GI_{50} level. It displayed high selectivity towards CNS subpanel, prostate subpanel and leukemia with selectivity ratios of 22.30, 15.38 and 12.56 at GI_{50} level respectively. It exhibited moderate selectivity against colon subpanel with selectivity ratio of 4.65 at GI_{50} level, while it was non-selectivity toward the NSCLC (selectivity ratio; 0.46), melanoma (selectivity ratio; 0.77), ovarian cancer (selectivity ratio; 0.54), renal cancer (selectivity ratio; 0.61) and breast cancer (selectivity ratio; 0.61) as shown in **Table S2** and **Figure 2** in comparison with monastrol.

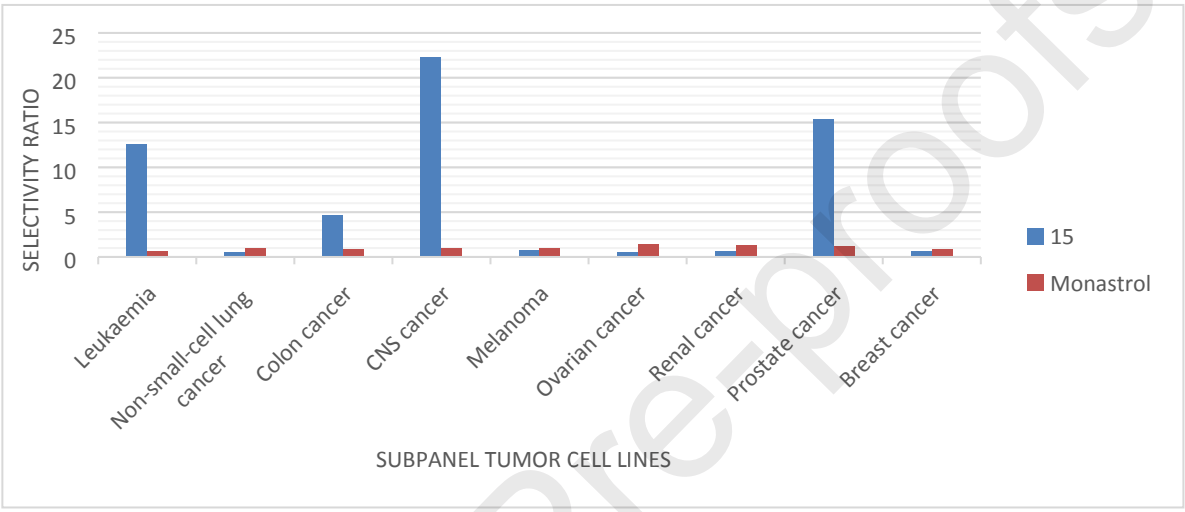

Figure 2. Subpanel tumor cell lines selectivity ratios of compound **15** and monastrol at GI_{50} level

The mean-graph midpoint (MG-MID) GI_{50} values comparison between compound **15** and monastrol as a standard are given in **Table 2**. It can be remarked that compound **15** displayed, comparatively superior activity over monastrol where, the data indicated that the MID for compound **15**, (8.92 µM) was a lot less than that of the MID (50.10 µM) calculated for monastrol (**Table 2**).

Table 2. Comparison of compound **15** with monastrol at MG-MID GI_{50} level at the five doses

Compound	L	NSCLC	CC	CNSC	M	OC	RC	PC	BC	MG-MID
15	0.71	19.21	1.92	0.4	11.64	16.52	14.67	0.58	14.67	8.92
Monastrol	30.52	48.03	41.94	49.27	48.57	66.99	62.76	59.6	43.24	50.10

Dose response curves (percentage growth verses concentration of compound at NCI protocol, µM) compound **15** against entirely cell lines in the NCI 60 panel are given in **Figures 3** and **S69**.

Colors-codes of different cancer cell lines: red, leukemia cell line; blue, lung cancer; green, colon cancer; gray, central nervous system cancer; coral, melanoma; purple, ovarian cancer; gold, renal cancer; turquoise, prostate cancer; pink, breast cancer.

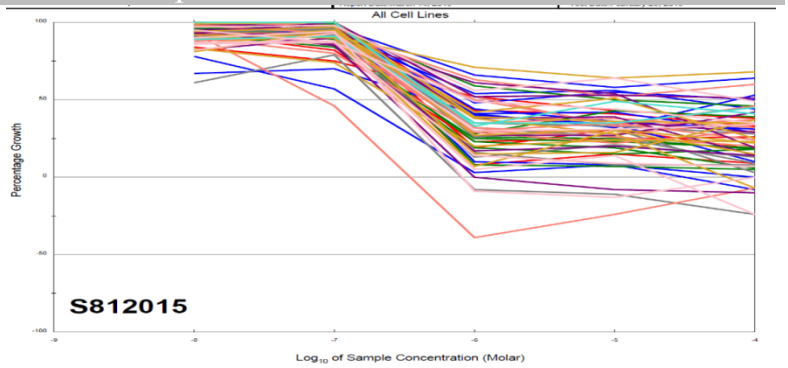

Figure 3. Collective dose response curves for entirely cell lines in the NCI 60 panel exposed to compound **15** (NSC 812015) with tissue originated colors.

3.2.2. Kinesin enzyme inhibition assay

Our synthesized target compounds were designed as inhibitors of kinesin enzyme which would lead to cell cycle arrest at mitosis and ultimately, to cell death. Consequently, the kinesin enzymatic assays for the most active DHPM derivatives were achieved, using monastrol and the potent inhibitor, mon-97 as references. The five selected compounds **9d**, **10b**, **12**, **15** and **16** exhibited higher inhibitory activity, in micro molar range (IC_{50} values from 3.86 to 14.07 μM), in comparison to the positive control, monastrol, which reported (IC_{50} = 20 μM), as indicated in **Table 3**. Consequently, we can conclude that the introduction of sulfur atom at the 2-position and the 1,3-benzodioxole moiety at position 4 were contributed to enhance the inhibitory activity of the DHPM scaffold as observed for all five tested compounds. The presence of phenyl group at the side chain at 5-position remarkably, initiated the inhibitory activity of compounds, **9d**, **10b** and **15**. In addition, benzimidazole analogues reported superior activity (compound **15**). Interestingly, the dimethyl cyclohexyl hydrophobic moiety lead to the most potent inhibitor, compound **12**, with IC_{50} = 3.95 μM surpassing that of all other tested compounds as well as the positive controls, monastrol and mon-97. Compound **9d** displayed 'cell drop-off' (i.e., lower potency in the cellular assay than in the enzyme assay) while it was the most potent inhibitor of kinesin with IC_{50} of 3.86 ± 0.12 μM (**Table 3**), it displayed poor biochemical efficacy towards mitotic kinesin target with MG-MID = 81.67 (**Table 1**). Science most known drug targets and metabolizing enzymes are located inside cells, compound **9d** could be metabolized rapidly or bind to other proteins outside or inside the cell cultures leading to its poor intracellular bioavailability and activity [41].

Table 3. Kinesin enzyme inhibitory activity for compounds **9d**, **10b**, **12**, **15** and **16**.

Compound	IC_{50}[a] ± SD[b] (μM)
9d	3.86 ± 0.12
10b	10.70 ± 0.35
12	3.95 ± 0.12
15	4.36 ± 0.14
16	14.07 ± 0.45
Monastrol	20 ± 0.42
Mon-97	0.1 ± 0.02

[a]The half maximal inhibitory concentration, [b]the standard deviation of triplicate experiments

3.2.3. In vitro cytotoxicity against human normal cell (Human Embryonic Kidney)

To investigate whether the synthesized compounds showed selective cytotoxicity between normal and cancer cells, the most active target compounds **9d, 10b, 12, 15** and **16** were evaluated against human embryonic kidney (HEK 293); a human normal cell line. As displayed in **Table 4**, all tested compounds **9d, 10b, 12, 15** and **16** exhibited lower toxicity towards normal cell, HEK 293, with IC_{50} = 27.99, 62.02, 33.20, 16.75 and 19.30 μM/ml respectively in comparison to doxorubicin as a reference drug (IC_{50} = 11.34 μM/ml). On the basis of this preceding information, the safest compound among test compounds on HEK 293 is **10b** about 5 times than doxorubicin. The representative IC_{50} values and curves showed in the SI in **Table S3** and **Figures S70-S75**.

Table 4. Cytotoxic activity (IC_{50}) of **9d, 10b, 12, 15** and **16** against human embryonic kidney normal cell (HEK 293)

Compound	IC_{50}[a] ± SD[b] (μM/ml)
9d	27.99 ± 1.09
10b	62.02 ± 2.42
12	33.20 ± 1.29
15	16.75 ± 0.65
16	19.30 ± 0.76
Doxorubicin (DOX)	11.34 ± 0.44

[a]The half maximal inhibitory concentration, [b]the standard deviation of triplicate experiments

3.2.4. Cell cycle analysis

Targeting the cancer cell cycle has been emerged as a promising approach for cancer therapy [42]. To recognize the role of compound **15** in growth inhibition of cancer cells, and consequently, induction of apoptosis in different phases, DNA flow cytometric analysis was used to measure the effect of compound **15** and monastrol on induction of cell cycle of SNB-75 cancer cells. SNB-75 cells were treated with compound **15** and monastrol at IC_{50} concentration (2 μM) for 24 h, stained with propidium iodide (PI), analyzed by flow cytometer and the results were reported in **Table 5**. A significant increase in the percentage of apoptotic cells at the pre-G1 phase, (24.82% on exposure to **15** and 22.58% for monastrol) compared to control (1.85%), was detected with concurrent reduction in the G0/G1 phase, 34.52% for **15** & 29.56% for monastrol, and compared to the control (55.62%). Furthermore, a significant increase in the cells at G2/M phase, 37.59% for **15** & 41.26%

for monastrol, was detected compared to control (10.46%) as shown in **Figure 4A**. Both arrest of G0/G1 phase and alteration of the pre-G1 phase are considered significant remarks for compound **15** to induce apoptosis in SNB-75 cells.

Table 5. Effect of compound **15** and monastrol on the cell cycle phases in SNB-75 cells.

Compound	Cell cycle distribution (%)			
	G0-G1	S	G2-M	pre-G1
15	34.52	27.89	37.59	24.82
Monastrol	29.56	29.18	41.26	22.58
Control	55.62	33.92	10.46	1.85

3.2.5. Detection of apoptosis

Extrinsic as well as intrinsic apoptosis in SNB-75 cells induced by compound **15** were evaluated by annexin V and PI staining. Herein, SNB-75 cells were incubated with compound **15** and monastrol at 2 µM concentration for 24 h. Compound **15** induced an early apoptosis, (7.65%), in SNB-75 at 24 h compared to monastrol (4.72%) and enhanced late apoptotic induction, (15.12%) by more than 25-fold over the untreated cells (0.59). Thus, compound **15** induced apoptosis with 22.77%, and the results were compared with monastrol (20.26%) (**Figure 4B**). This determination was consistent with the data obtained from cell cycle analysis in **Figure 4A**.

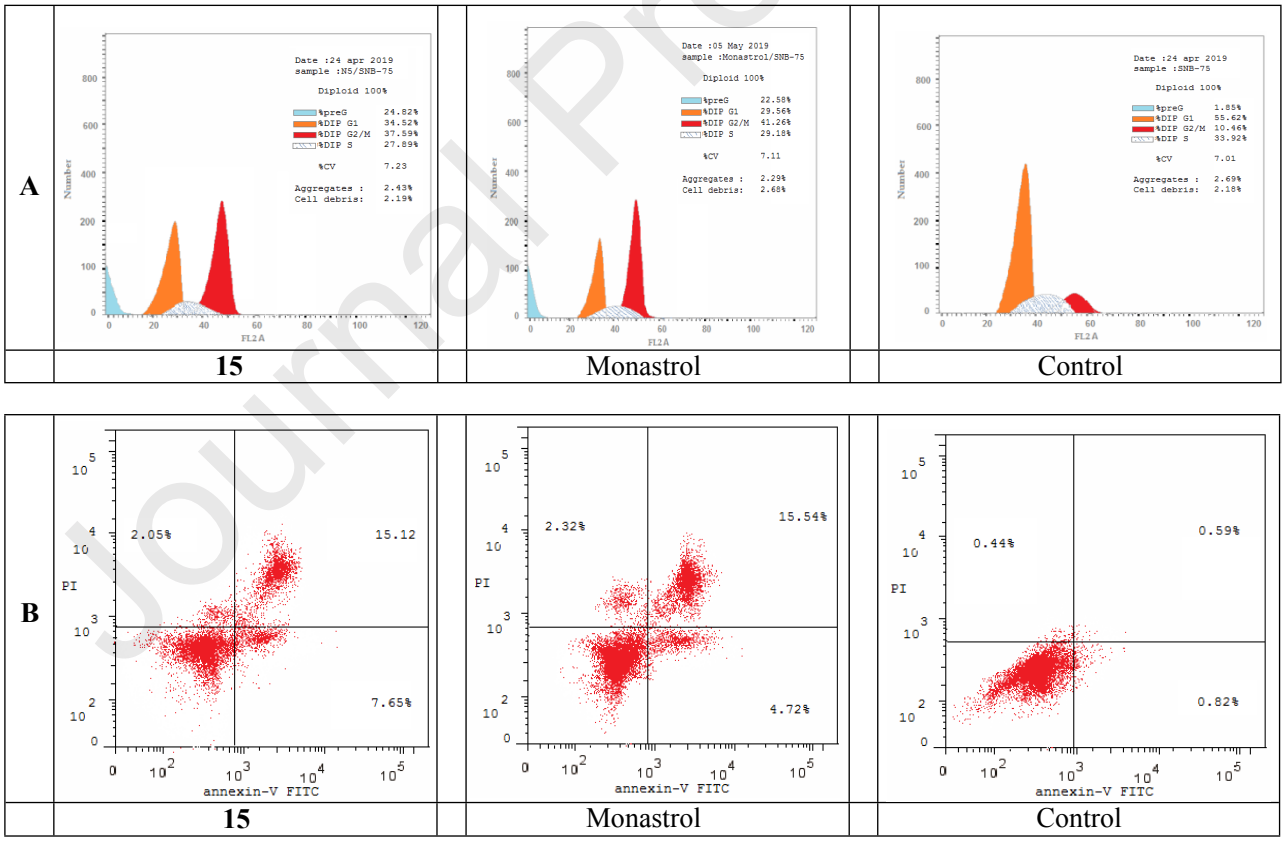

Figure 4. A) Effect of compound **15** on the cell cycle distribution of SNB-75 cell line. **B)** Apoptosis effect on SNB-75 cell line induced by compound **15**, the four quadrants identified as: LL: viable; LR: early apoptotic; UR: late apoptotic; UL: necrotic.

3.2.6. Effects on the levels of active caspase-3 and caspase-9

Caspases, cysteine-containing aspartic acid-specific proteases, provide essential links in cell controlling networks regulatory cell death. Caspase-3 is a crucial executioner protease which is triggered by upstream initiator caspases as caspase-9 [43, 44].

This study was further extended to investigate the ability of compounds **9d** and **15** to provoke apoptosis in MDA-MB-435 melanoma cell line. Treatment of MDA-MB-435 cell line with compound **9d** significantly increased the expression levels of active caspases 3 and 9 by about 7 and 18 folds, respectively, while in case of compound **15** the levels of active caspases-3 and caspases-9 increased considerably by about 6 and 12 folds, respectively, in comparison to the control. Interestingly, compound **9d** displayed superior effect on both caspase-3 and caspases-9 over monastrol as indicated in **Table 6**.

Table 6. Effect of compounds **9d** and **15** on the active caspase-3 and caspase-9 level in MDA-MB-435 cells.

Compound	Caspase-3		Caspase-9	
	Pg/ml	Fold	ng/ml	Fold
9d	354.20	7.90	22.12	18.79
15	306.20	6.83	14.63	12.43
Monastrol	309.20	6.90	14.03	11.92
Control	44.80	1	1.18	1

3.3. Molecular docking

We have designed and synthesized novel series of DHPM as inhibitors of mitotic kinesin Eg5. In order to understand the protein-ligand interaction, we have performed molecular docking studies using AutoDock Vina [45] and UCSF Chimera (version 1.13.1) programs.

Kinesin is composed of an N-terminal motor domain bound through a linker to a central coiled-coil and a C-terminal tail. The motor domain interacts with microtubules, and it is also responsible for ATP hydrolysis and force generation [46, 47]. The allosteric binding site of Eg5 has been studied through molecular modeling techniques and has been found to contain three hydrophobic sub pockets (P1–P3) which interact with the inhibitors [48-51].

some demonstrative compounds, **9d**, **10b**, **12**, **15**, **16** and monastrol were docked into the crystal structure of Eg5 motor domain, (PDB ID code 1Q0B) [48] allosteric binding site and the best poses were evaluated by docking energy score values and their alignment with co-crystalized monastrol were shown in **Figures S76-81**. Docking of R- and S-enantiomers of selected compounds revealed that S-enantiomers exhibited better interaction and affinity than R- enantiomers as shown in **Table S4**. Analysis of the molecular docking results showed that the interactions within the active site were attributed to hydrogen bonds, hydrophobic and electrostatic attraction forces. Compounds **9d**, **10b**, **12**, **15**, and **16** were fitted well into the allosteric binding site. The resulted molecular docking files were analyzed using Discovery Studio (DS) visualizer program [52] and the docking results were

reported in **Table 7**.

Table 7. Analysis of binding interaction of S-enantiomers of **9d**, **10b**, **12**, **15**, **16** and monastrol with KSP allosteric binding site

Compound code	IC_{50} (μM)	Hydrogen bonding interaction	Hydrophobic interaction	Electrostatic interaction
9d	3.86	Gly117, Arg221	Thr112, Glu118, Arg119, Ile136, Leu160, Tyr211, Leu214, Glu215, Gly217, Ala218, Arg221, Phe239	Glu116, Arg221
10b	10.70	Glu116, Gly117	Glu118, Arg119, Ile136, Pro137, Leu160, Tyr211, Leu214, Gly217, Ala218, Arg221, Phe239	Glu116
12	3.95	Glu116, Gly117	Thr112, Glu118, Arg119, Ile136, Pro137, Leu160, Tyr211, Leu214, Glu215, Gly217, Ala218, Phe239	Glu116, Arg221
15	4.36	Tyr211	Thr112, Gly117, Glu118, Arg119, Ile136, Pro137, Leu160, Tyr211, Leu214, Glu215, Ala218, Arg221, Phe239	Glu116
16	14.07	Gly117	Thr112, Glu118, Arg119, Ile136, Pro137, Leu214, Ala218, Arg221	Glu116
Monastrol	20	Glu116, Glu118	Gly117, Arg119, Ile136, Tyr211, Leu214, Glu215, Ala218	none

The most active analogue, **9d**, forms two H-bonds, one with the back bone carbonyl oxygen of Gly117 in the allosteric binding pocket. The second H-bond is formed with the proton of the NH_2 of Arg221 located in a minor cooperative binding pocket [53]. Moreover, it develops electrostatic attraction forces, aromatic π-anion and π-cation interactions, with two amino acid residues, Glu116 and Arg221 respectively. Besides, strong hydrophobic interactions between aromatic rings with various hydrophobic amino acid residues have been confirmed as shown in **Figure 5**. There was a minor cooperative binding pocket surrounded by Ala218 and Arg221.

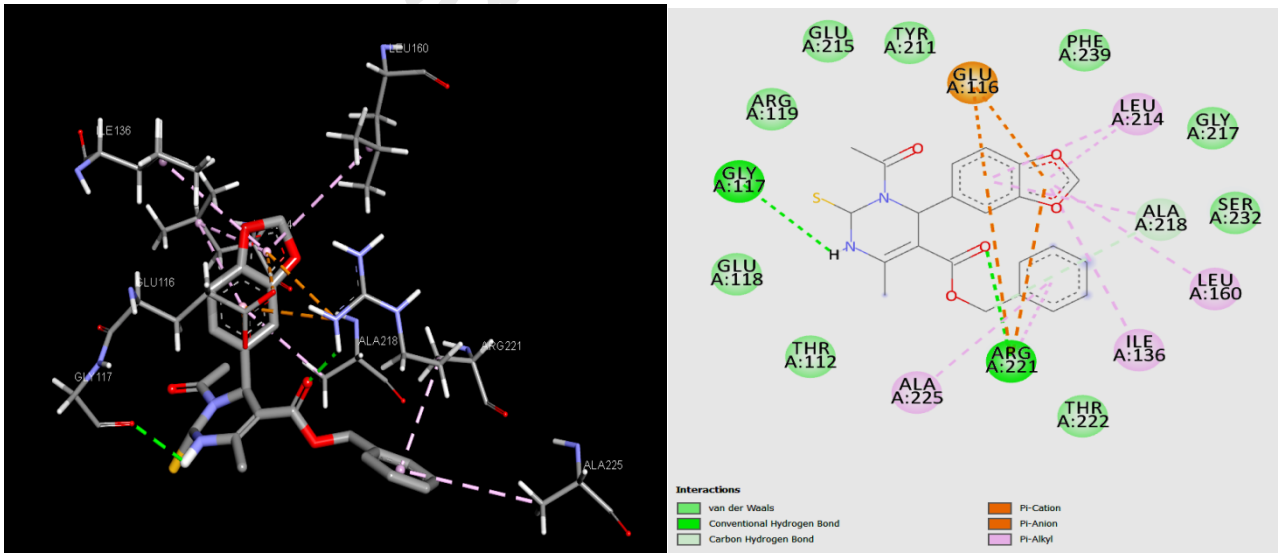

Figure 5. The 2D (right) and 3D (left) of the best docked poses showing interactions of S-enantiomer of **9d** with the amino acids of the active site of KSP.

The observed lower biological activity of analogue, **10b**, could be explained by forming only one H-bond with either the carbonyl group of the nearby amino acid residues, Glu116 or Gly117. In addition,

it has only one electrostatic aromatic π-anion interaction with the acidic amino acid Glu116 as presented in **Figure 6**.

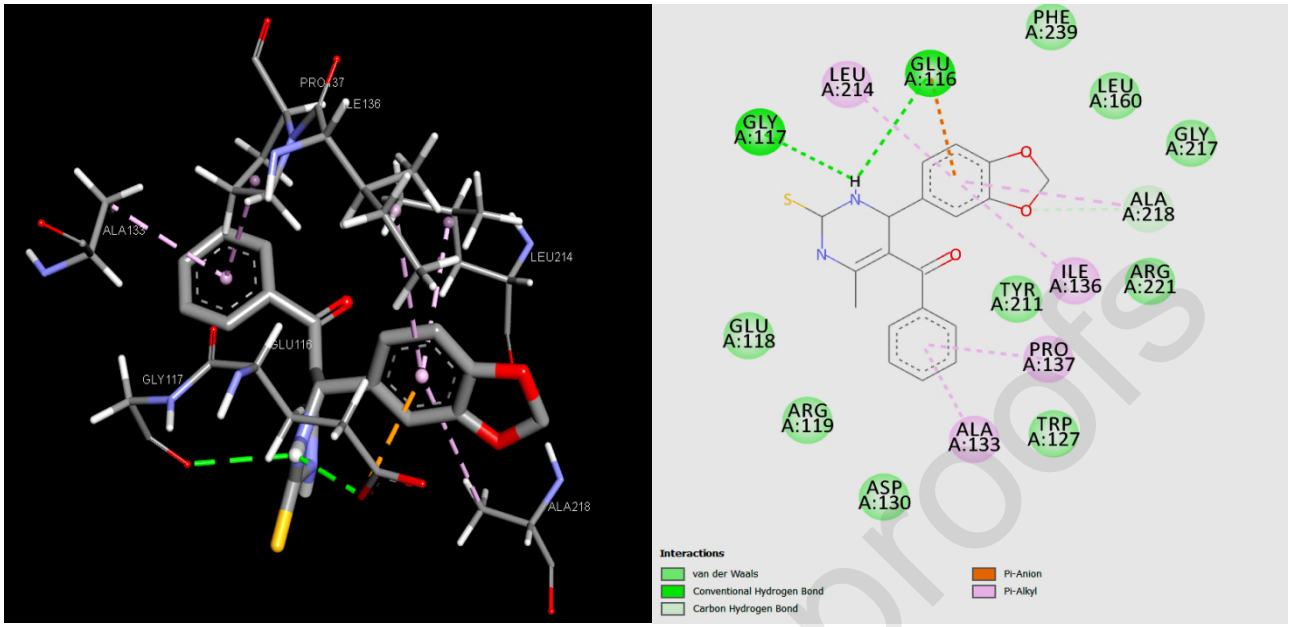

Figure 6. The 2D (right) and 3D (left) of the best docked poses showing interactions of S-enantiomer of **10b** with the amino acids of the active site of KSP.

The high potency of compound **12**, could be explained by the additional hydrophobic π-alkyl attraction forces between the two methyl groups located in the cyclohexanone ring with Ala218 and Arg119. Furthermore, the electrostatic aromatic π-anion and π-cation interactions with the amino acid residues, Glu116 and Arg221 were established (**Figure 7**).

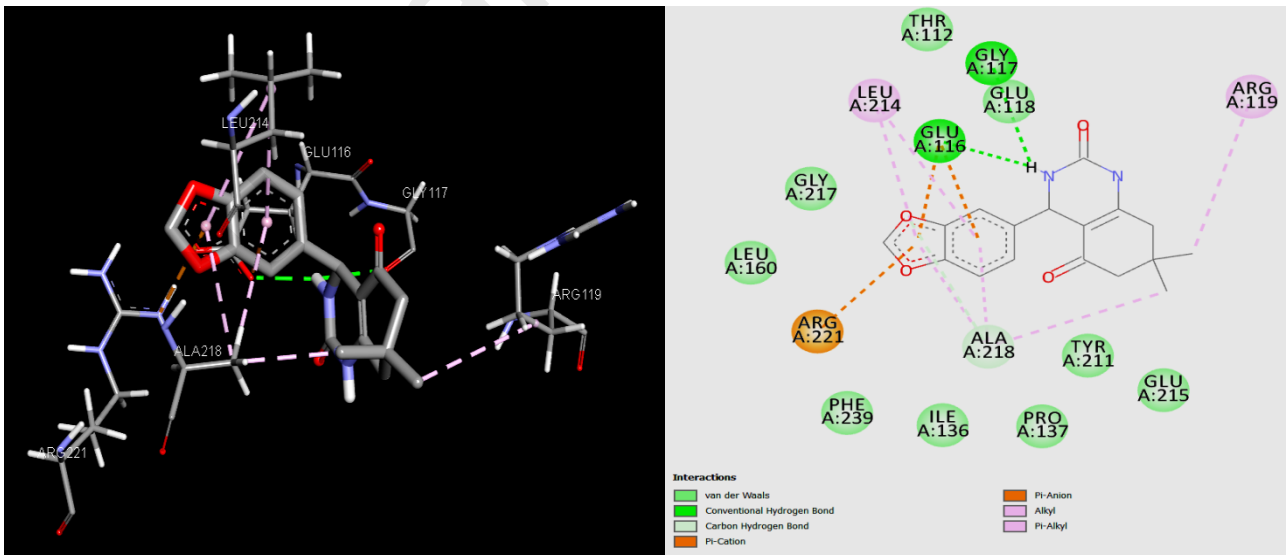

Figure 7. The 2D (right) and 3D (left) of the best docked poses showing interactions of S-enantiomer of **12** with the amino acids of the active site of KSP.

The relatively high activity of compound **15** is elucidated by the unique H-bond formed between the benzimidazole-nitrogen and the proton of the hydroxyl group of Tyr211 in addition to the

hydrophobic attraction forces between benzyl ester with Ile136 and Leu214. It forms hydrophobic aromatic π-anion interaction with Glu116. Furthermore, a face to face aromatic π-π- stacking of benzimidazole ring with the benzene ring of Tyr211 is confirmed as shown in **Figure 8**.

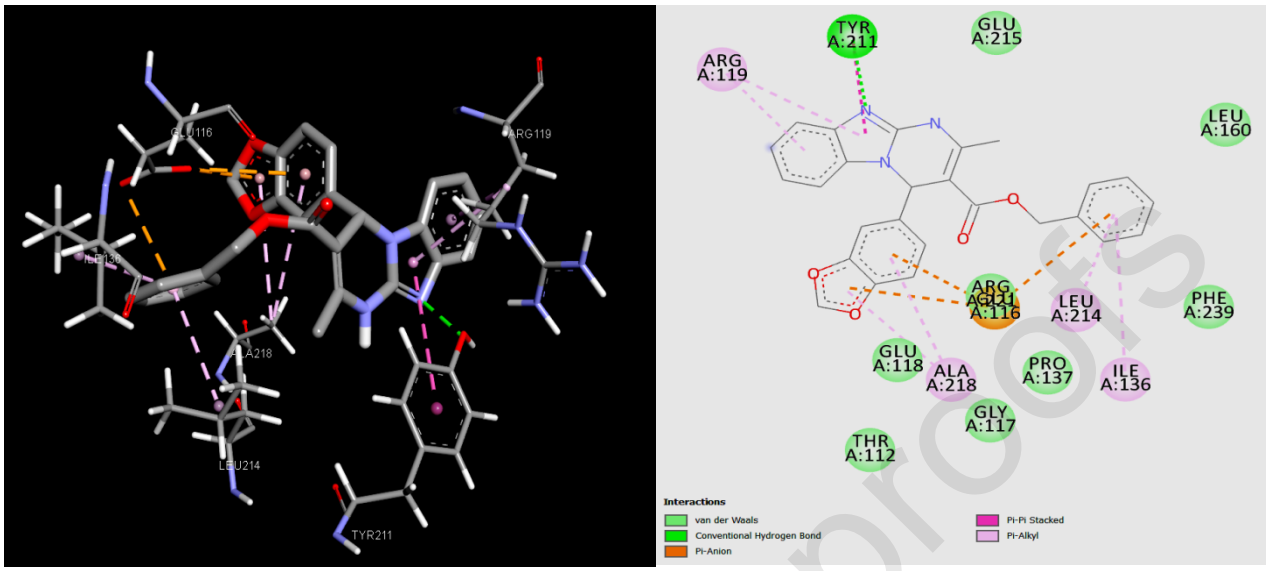

Figure 8. The 2D (right) and 3D (left) of the best docked poses showing interactions of S-enantiomer of **15** with the amino acids of the active site of KSP.

Compound **16**, has relatively low potency compared to analogue **15** because of the absence of the benzyl ester side chain and consequently the hydrophobic interaction with the corresponding amino acid residues in the active site. Moreover, it lost the π-π stacking as well as the H-bond between benzimidazole ring and Tyr211. It forms only one H-bond with Gly117 as well as electrostatic aromatic π-anion interaction with Glu116. Weaker hydrophobic interactions with hydrophobic nearby amino acid were also informed (**Figure 9**)

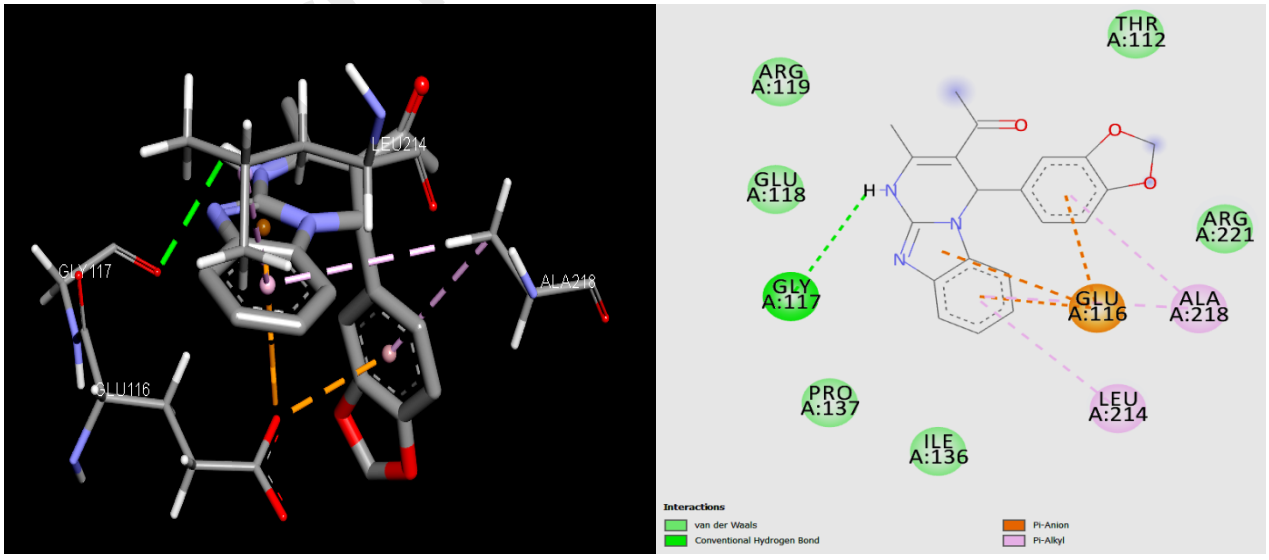

Figure 9. The 2D (right) and 3D (left) of the best docked poses showing interactions of S-enantiomer of **16** with the amino acids of the active site of KSP

Besides the observed attraction forces of the selected compounds with the main binding pocket, there was a minor cooperative binding pocket surrounded by Ala218 and Arg221. Binding to the latter pocket enhanced the binding affinity of the studded compounds compared to those reported for monastrol (**Table 7**).

4. Conclusion

In this study, novel series of twenty-one DHPM derivatives were designed and synthesized according to Biginelli method. The anticancer activity of all of these derivatives, were tested at a single dose of 10^{-5} M concentration at the NCI (USA) over 60 cell line panel, and DHPM hybrid with benzimidazole moiety **15** was subsequently tested in 5-doses testing mode. Hybrid **15** was identified as the most promising anticancer candidate against most of cell lines. The inhibitory activity against kinesin enzyme was also investigated for selected compounds **9d**, **10b**, **12**, **15** and **16** with IC_{50} ranges, 3.86 - 14.07 μM (exceed monastrol). Compound **9d** exhibited the best inhibitory activity with IC_{50} value at 3.86 μM. The safest compound among test compounds on normal cell line (HEK 293) is **10b** (IC_{50} = 62.02 ± 2.42 μM/ml) about 5 times than doxorubicin. Flow cytometric analysis indicated that the SNB-75 cells were arrested in G2/M phase by compound **15**. The effects of compounds **9d** and **15** on the active caspase-3 and caspase-9 levels were also investigated. The most active kinesin inhibitors, **9d**, **10b**, **12**, **15** and **16** were docked into the kinesin Eg5 binding site, which developed significant attraction forces with various amino acid residues in the active site better than monastrol. The DHPM analogues discovered in this study may provide valuable therapeutic intervention for cancer treatment.

5. Experimental

5.1. Chemistry

5.1.1. General

All organic reagents used were obtained from Sigma-Aldrich company, Alfa Aesar company or Merck company and were used without further purification. All potential Eg5 inhibitors were synthesized in their racemic form (±) using the well-known Biginelli three component reaction. The optical rotations (α) of all synthesized compounds were recorded on a Polax-2L Polarimeter (ATAGO Co., Ltd., Japan) at the department of pharmaceutical chemistry, Faculty of Pharmacy, Tanta University, Egypt and they didn't show a rotation. Melting points were determined on an electro-thermal melting point apparatus (Stuart SMP10) by the open capillary method and were reported uncorrected. Reactions were monitored by TLC using pre-coated sheet (Fastman Kodak Co., Silica 60 F_{254}) using developing systems: n-hexane: ethyl acetate (40: 60) and were visualized with UV light at 254 nm. Elemental analysis (% C, H, N, and S) was carried out by Perkin–Elmer 2400 CHNS analyzer and were within ± 0.40 of the theoretical values. Elemental analysis was performed by the

regional center for mycology and biotechnology, Al-Azhar University, Nasr City, Cairo, Egypt. ^{1}H, ^{13}C NMR, DEPT-135, 2D COSY and HSQC spectra were recorded on Bruker FT-NMR spectrometer at (400 MHz) and (100 MHz) respectively using DMSO-d_6 as a solvent. A mixture of DMSO-d_6 and DMF was used to dissolve compounds **10b** and **10d**. All chemical shift values, coupling constants, *J*, and multiplicity (s = singlet, d = doublet, t = triplet, m = multiplet, br = broad, dd = doublet of doublet) were quoted in ppm and in Hz respectively. ^{1}H and ^{13}C NMR spectra were performed by Faculty of Pharmacy, Mansoura University, Egypt. Electron ionization mass spectra (EI-MS) were recorded on Thermo Scientific, ISQ Single Quadruple MS, with ionization energy of 70 eV, and Helium gas was used as the carrier gas at a constant flow rate of 1ml/min. Mass spectroscopy was performed by the regional center for mycology and biotechnology, Al-Azhar University, Nasr City, Cairo, Egypt.

5.1.2. 1,3-Benzodioxole-5-carbaldehyde (Piperonal) **4**

A solution of 3,4-dihydroxybenzaldehyde **3** (5.0 g, 36 mmol) in DMF (25 ml) was added dropwise to a suspension of dichloromethane (3.5 ml, 54 mmol) and potassium carbonate (10 g, 72 mmol) in DMF (25 ml). The mixture was heated under reflux for 12 h then cooled and filtered. The filtrate was evaporated under vacuum. The remaining residue was dissolved in water and then extracted with diethyl ether (3 x 30 ml). The ethereal extracts were collected, washed with sodium hydroxide (30 ml, 10 %) followed by distilled water (30 ml), dried over anhydrous magnesium sulfate and finally the ether layer was evaporated under vacuum. The formed precipitate was crystallized from EtOH to give compound **4** (3.5 g, 65%) as a light yellow solid with m.p. 37-39 ^{o}C (Lit. m.p. 35-39 ^{o}C) [30, 31].

5.1.3. General procedure for preparation of acetoacetic esters derivatives **(6a-d)**

A solution of the appropriate alcohol, **5a-d**, (25 mmol) and TMD (3.5 g, 25 mmol) in 10 ml xylene was heated under reflux in an oil bath at 150 ^{o}C, for 6 h. The reaction mixture was cooled and then xylene was removed under reduced pressure to yield products, **6a-d** which were in a high level of purity and were used immediately in subsequent reactions [34]. **6a**, a yellow oil, with bp 183-185 ^{o}C, (Lit. bp 185-187 ^{o}C), **6b**, a yellow oil, with bp 200-201 ^{o}C, (Lit. bp 204-205 ^{o}C), **6c**, a yellow oil, with bp 115-117 ^{o}C, (Lit bp 120-122 ^{o}C) and **6d**, a yellow oil, with bp 270-271 ^{o}C, (Lit bp 275-276 ^{o}C) [54].

5.1.4. General procedure for preparation of DHPM compounds **(8a–h)**

A mixture of acetoacetate esters **6a-d** (25 mmol), compound **4** (25 mmol), thiourea **7a** / urea **7b** (50 mmol), citric acid (25 mmol) and triethylorthoformate (50 mmol) was heated under reflux for 10 h. The reaction was quenched by addition of water (15 ml) and then cooled in an ice-bath. The precipitated solid was filtered, and recrystallized from isopropanol to afford products (**8a-h**).

5.1.4.1. (±)-*isopropyl 4-(benzo[d][1,3]dioxol-5-yl)-6-methyl-2-thioxo-1,2,3,4-tetrahydro-*

pyrimidine-5- carboxylate **(8a)**

Yield (0.23 g, 66 %) as white powder with m.p. 175-176 ^{o}C. ^{1}H NMR (400 MHz, DMSO-d_6) δ (ppm): 1.03 (3H, d, *J* = 6.0 Hz, $CHCH_3$), 1.18 (3H, d, *J* = 6.0 Hz, $CHCH_3$), 2.29 (3H, s, CH_3), 4.84 – 4.87 (1H, m, COOCH), 5.08 (1H, d, *J* = 1.6 Hz, pyrimidine 4-H), 6.01 (2H, s, OCH_2O), 6.68 (1H, dd, *J* = 8.0, 1.6 Hz, 6-H), 6.73 (1H, d, *J* = 1.6 Hz, 4-H), 6.89 (1H, d, *J* = 8.0 Hz, 7-H), 9.59 (1H, d, *J* = 1.6 Hz, 3-NH) , 10.29 (1H, s, 1-NH). ^{13}C NMR (100 MHz, DMSO) δ (ppm): 17.57, 21.93, 22.18, 54.24, 67.32, 101.46, 101.54, 107.20, 108.57, 120.17, 138.05, 145.25, 147.13, 147.81, 165.06, 174.45. EI-MS: *m/z*: 334.02 [M^+]. Anal. Calcd. for $C_{16}H_{18}N_2O_4S$: C, 57.47; H, 5.44; N, 8.38; S, 9.59. Found: C, 57.67; H, 5.56; N, 8.68; S, 9.77.

5.1.4.2. (±)-*isobutyl 4-(benzo[d][1,3]dioxol-5-yl)-6-methyl-2-thioxo-1,2,3,4-tetrahydro-pyrimidine-5-carboxylate* **(8b)**

Yield (0.19 g, 53 %) as faint yellow powder with m.p. 134 -135 ^{o}C. ^{1}H NMR (400 MHz, DMSO-d_6) δ (ppm): 0.77-0.78 (6H, m, $CH(CH_3)_2$), 1.75 – 1.81 (1H, m, $CH(CH_3)_2$), 2.33 (3H, s, CH_3), 3.74 (1H, dd, *J* = 10.8, 6.4 Hz, $COOCH_2$), 3.81 (1H, dd, *J* = 10.8, 6.4 Hz, $COOCH_2$), 5.11 (1H, d, *J* = 2.8 Hz, pyrimidine 4-H), 5.99 (2H, s, OCH_2O), 6.69 (1H, dd, *J* = 8.0, 1.6 Hz, 6-H), 6.74 (1H, d, *J* = 1.6 Hz, 4-H), 6.88 (1H, d, *J* = 8.0 Hz, 7-H), 9.59 (1H, d, *J* = 2.8 Hz, 3-NH) , 10.33 (1H, s, 1-NH). ^{13}C NMR (100 MHz, DMSO) δ (ppm): 17.67, 19.27, 19.33, 27.68, 54.17, 70.04, 100.81, 101.55, 107.23, 108.66, 120.17, 137.72, 145.94, 147.20, 147.90, 165.57, 174.33. EI-MS: *m/z*: 348.01 [M^+]. Anal. Calcd. for $C_{17}H_{20}N_2O_4S$: C, 58.60; H, 5.80; N, 8.04; S, 9.20. Found: C, 58.60; H, 5.52; N, 7.98; S, 8.99.

5.1.4.3. (±)-*2-methoxyethyl 4-(benzo[d][1,3]dioxol-5-yl)-6-methyl-2-thioxo-1,2,3,4-tetrahydro-pyrimidine-5-carboxylate* **(8c)**

Yield (0.25 g, 69 %) as faint yellow powder with m.p. 179 -181 ^{o}C. ^{1}H NMR (400 MHz, DMSO-d_6) δ (ppm): 2.29 (3H, s, CH_3), 3.22 (3H, s, OCH_3), 3.45-3.50 (2H, m, CH_2OCH_3), 4.05-4.17 (2H, m, $COOCH_2$), 5.11 (1H, d, *J* = 2.8 Hz, pyrimidine 4-H), 6.00 (2H, s, OCH_2O), 6.70 (1H, dd, *J* = 8.0, 1.6 Hz, 6-H), 6.75 (1H, d, *J* = 1.6 Hz, 4-H), 6.88 (1H, d, *J* = 8.0 Hz, 7-H), 9.62 (1H, d, *J* = 2.8 Hz, 3-NH), 10.36 (1H, s, 1-NH). ^{13}C NMR (100 MHz, DMSO) δ (ppm): 17.61, 54.06, 58.43, 63.14, 70.24, 101.13, 101.54, 107.20, 108.64, 120.02, 137.95, 145.75, 147.15, 147.84, 165.48, 174.65. EI-MS: *m/z*: 349.96 [M^+]. Anal. Calcd. for $C_{16}H_{18}N_2O_5S$: C, 54.84; H, 5.19; N, 8.00; S, 9.15. Found: C, 54.97; H, 5.45; N, 8.20; S, 9.43.

5.1.4.4. (±)-*benzyl 4-(benzo[d][1,3]dioxol-5-yl)-6-methyl-2-thioxo-1,2,3,4-tetrahydropyrimidine-5-carboxylate* **(8d)**

Yield (0.28 g, 71 %) as yellow powder with m.p. 202-204 ^{o}C, (Lit. m.p. 204 ^{o}C) [15]. ^{1}H NMR (400 MHz, DMSO-d_6) δ (ppm): 2.33 (3H, s, CH_3), 5.03 (1H, d, *J* = 12.4 Hz, $COOCH_2$), 5.12 (1H, d, *J* = 12.4 Hz, $COOCH_2$), 5.14 (1H, d, *J* = 1.6 Hz, pyrimidine 4-H), 6.01 (2H, s, OCH_2O), 6.66 (1H, dd, *J*

= 8.0, 1.6 Hz, 6-H), 6.71 (1H, d, *J* = 1.6 Hz, 4-H), 6.86 (1H, d, *J* = 8.0 Hz, 7-H), 7.17 – 7.33 (5H, m, Bn-H_5), 9.62 (1H, d, *J* = 1.6 Hz, 3-NH), 10.37 (1H, s, 1-NH). ^{13}C NMR (100 MHz, DMSO) δ (ppm): 17.71, 54.18, 65.59, 100.63, 101.58, 107.33, 108.64, 120.24, 128.06, 128.29, 128.77, 136.74, 137.77, 146.30, 147.24, 147.89, 165.32, 174.36. EI-MS: *m/z*: 382.02 [M^+]. Anal. Calcd. for $C_{20}H_{18}N_2O_4S$: C, 62.81; H, 4.75; N, 7.33; S, 8.39. Found: C, 62.56; H, 4.54; N, 7.09; S, 8.55.

5.1.4.5. (±)-*isopropyl 4-(benzo[d][1,3]dioxol-5-yl)-6-methyl-2-oxo-1,2,3,4-tetrahydropyrimidine-5-carboxylate* **(8e)**

Yield (0.28 g, 85 %) as white powder with m.p. 192-193 °C, (Lit. m.p. 194-196 °C) [55]. ^{1}H NMR (400 MHz, DMSO-d_6) δ (ppm): 1.02 (3H, d, *J* = 6.4 Hz, $CHCH_3$), 1.17 (3H, d, *J* = 6.4 Hz, $CHCH_3$), 2.25 (3H, s, CH_3), 4.80 – 4.85 (1H, m, COOCH), 5.07 (1H, s, pyrimidine 4-H), 5.99 (2H, s, OCH_2O), 6.70 (1H, d, *J* = 8.0 Hz, 6-H), 6.75 (1H, s, 4-H), 6.86 (1H, d, *J* = 8.0 Hz, 7-H), 7.67 (1H, s, 3-NH) , 9.15 (1H, s, 1-NH). ^{13}C NMR (100 MHz, DMSO) δ (ppm): 18.18, 21.98, 22.25, 54.21, 66.79, 100.02, 101.39, 107.14, 108.41, 119.86, 139.46, 146.77, 147.67, 148.51, 152.51, 165.28. EI-MS: *m/z*: 318.16 [M^+]. Anal. Calcd. for $C_{16}H_{18}N_2O_5$: C, 60.37; H, 5.71; N, 8.80. Found: C, 60.03; H, 5.72; N, 8.65.

5.1.4.6. (±)-*isobutyl 4-(benzo[d][1,3]dioxol-5-yl)-6-methyl-2-oxo-1,2,3,4-tetrahydropyrimidine-5-carboxylate* **(8f)**

Yield (0.24 g, 70 %) as white powder with m.p. 181-183 °C. ^{1}H NMR (400 MHz, DMSO-d_6) δ (ppm): 0.78 (6H, d, *J* = 5.2 Hz, $CH(CH_3)_2$), 1.75 – 1.80 (1H, m, $CH(CH_3)_2$), 2.29 (3H, s, CH_3), 3.72 (1H, d, *J* = 6.2 Hz, $COOCH_2$), 3.77 (1H, d, *J* = 6.2 Hz, $COOCH_2$), 5.09 (1H, s, pyrimidine 4-H), 5.99 (2H, s, OCH_2O), 6.70 (1H, d, *J* = 7.6 Hz, 6-H), 6.75 (1H, s, 4-H), 6.86 (1H, d, *J* = 7.6 Hz, 7-H), 7.68 (1H, s, 3-NH) , 9.19 (1H, s, 1-NH). ^{13}C NMR (100 MHz, DMSO) δ (ppm): 18.27, 19.33, 19.37, 27.72, 54.11, 69.74, 99.39, 101.40, 107.13, 108.52, 119.80, 139.16, 146.83, 147.75, 149.24, 152.43, 165.79. EI-MS: *m/z*: 332.04 [M^+]. Anal. Calcd. for $C_{17}H_{20}N_2O_5$: C, 61.43; H, 6.08; N, 8.43. Found: C, 61.21; H, 6.31; N, 8.52.

5.1.4.7. (±)-*2-methoxyethyl 4-(benzo[d][1,3]dioxol-5-yl)-6-methyl-2-oxo-1,2,3,4-tetrahydro-pyrimidine -5-carboxylate* **(8g)**

Yield (0.30 g, 86 %) as white powder with m.p. 146 -148 °C. ^{1}H NMR (400 MHz, DMSO-d_6) δ (ppm): 2.25 (3H, s, CH_3), 3.23 (3H, s, OCH_3), 3.44 – 3.49 (2H, m, 8.8 Hz, CH_2OCH_3), 4.06 – 4.10 (2H, m, $COOCH_2$), 5.09 (1H, d, *J* = 3.2 Hz, pyrimidine 4-H), 5.98 (2H, s, OCH_2O), 6.72 (1H, dd, *J* = 8.0, 1.4 Hz, 6-H), 6.77 (1H, d, *J* = 1.4 Hz, 4-H), 6.85 (1H, d, *J* = 8.0 Hz, 7-H), 7.70 (1H, d, *J* = 3.2 Hz, 3-NH), 9.21 (1H, s, 1-NH). ^{13}C NMR (100 MHz, DMSO) δ (ppm): 18.23, 53.98, 58.43, 62.81, 70.34, 99.69, 101.39, 107.15, 108.49, 119.71, 139.33, 146.80, 147.70, 149.10, 152.62, 165.68. EI-MS: *m/z*: 334.00 [M^+]. Anal. Calcd. for $C_{16}H_{18}N_2O_6$: C, 57.48; H, 5.44; N, 8.38. Found: C, 57.76; H, 5.61; N, 8.22.

5.1.4.8. (±)*-benzyl 4-(benzo[d][1,3]dioxol-5-yl)-6-methyl-2-oxo-1,2,3,4-tetrahydropyrimidine-5-carboxylate* **(8h)**

Yield (0.30 g, 79 %) as white powder with m.p. 166-168 ^{o}C. ^{1}H NMR (400 MHz, DMSO-d_6) δ (ppm): 2.28 (3H, s, CH_3), 5.01 (1H, d, *J* = 12.8 Hz, $COOCH_2$), 5.09 (1H, d, *J* = 12.8 Hz, $COOCH_2$), 5.12 (1H, d, *J* = 2.6 Hz, pyrimidine 4-H), 5.99 (2H, s, OCH_2O), 6.68 (1H, dd, *J* = 8.0, 1.4 Hz, 6-H), 6.72 (1H, d, *J* = 1.4 Hz, 4-H), 6.83 (1H, d, *J* = 8.0 Hz, 7-H), 7.17 – 7.33 (5H, m, Bn-H_5), 7.70 (1H, d, *J* = 2.6 Hz, 3-NH), 9.25 (1H, s, 1-NH). ^{13}C NMR (100 MHz, DMSO) δ (ppm): 18.33, 65.24, 66.45, 99.17, 101.43, 107.24, 108.51, 119.89, 127.98, 128.19, 128.49, 128.74, 128.90, 137.01, 139.17, 146.88, 147.76, 149.73, 152.35, 165.51. EI-MS: *m/z*: 366.02 [M^+]. Anal. Calcd. for $C_{20}H_{18}N_2O_5$: C, 65.57; H, 4.96; N, 7.65. Found: C, 65.24; H, 4.81; N, 7.49.

5.1.5. General procedure for preparation of acetylated DHPM compounds **(9a–d)**

A solution of **8a-d** (5 mmol) in 15 ml of acetic anhydride was heated under reflux for 5 h. The solution was then poured into 150 ml of ice-water and stirred for 12 hours until complete precipitation of the product. The precipitate was filtered and then recrystallized from acetone to yield compounds **(9a-d).**

5.1.5.1. (±)*-Isopropyl 3-acetyl-4-(benzo[d][1,3]dioxol-5-yl)-6-methyl-2-thioxo-1,2,3,4-tetrahydro-pyrimidine -5-carboxylate* **(9a)**

Yield (0.22 g, 44 %) as yellow powder with m.p. 165-166 ^{o}C. ^{1}H NMR (400 MHz, DMSO-d_6) δ (ppm): 1.16 (3H, d, *J* = 6.0 Hz, $CHCH_3$), 1.22 (3H, d, *J* = 6.0 Hz, $CHCH_3$), 2.35 (3H, s, $COCH_3$), 2.63 (3H, s, CH_3), 4.95 – 4.98 (1H, m, COOCH), 6.00 (2H, s, OCH_2O), 6.31 (1H, s, pyrimidine 4-H), 6.66 (2H, m, 4,6-H_2), 6.87 (1H, d, *J* = 7.6 Hz, 7-H), 11.67 (1H, s, 1-NH). ^{13}C NMR (100 MHz, DMSO) δ (ppm): 16.93, 22.06, 22.12, 27.67, 53.01, 68.26, 101.67, 107.01, 108.07, 108.63, 120.13, 133.27, 145.11, 147.34, 147.89, 164.76, 173.55, 178.28. EI-MS: *m/z*: 376.17 [M^+]. Anal. Calcd. for $C_{18}H_{20}N_2O_5S$: C, 57.43; H, 5.37; N, 7.44; S, 8.52. Found: C, 57.01; H, 5.34; N, 7.19; S, 8.31.

5.1.5.2. (±)*-Isobutyl 3-acetyl-4-(benzo[d][1,3]dioxol-5-yl)-6-methyl-2-thioxo-1,2,3,4-tetrahydro-pyrimidine -5-carboxylate* **(9b)**

Yield (0.27 g, 66 %) as yellow crystal with m.p. 137 -138 ^{o}C. ^{1}H NMR (400 MHz, DMSO-d_6) δ (ppm): 0.82 (3H, d, *J* = 2.0 Hz, $CH(CH_3)$), 0.84 (3H, d, *J* = 2.0 Hz, $CH(CH_3)$), 1.78 – 1.90 (1H, m, $CH(CH_3)_2$), 2.37 (3H, s, $COCH_3$), 2.62 (3H, s, CH_3), 3.86 (1H, dd, *J* = 10.8, 6.4 Hz, $COOCH_2$), 3.90 (1H, dd, *J* = 10.8, 6.4 Hz, $COOCH_2$), 6.00 (2H, s, OCH_2O), 6.39 (1H, s, pyrimidine 4-H), 6.68 (1H, d, *J* = 8.0 Hz, 6-H), 6.70 (1H, s, 4-H), 6.87 (1H, d, *J* = 8.0 Hz, 7-H), 11.72 (1H, s, 1-NH). ^{13}C NMR (100 MHz, DMSO) δ (ppm): 16.86, 19.29, 19.32, 27.58, 27.70, 52.78, 70.54, 101.69, 107.19, 107.58, 108.64, 120.35, 132.96, 145.60, 147.41, 147.92, 165.12, 173.41, 178.28. EI-MS: *m/z*: 390.29 [M^+]. Anal. Calcd. for $C_{19}H_{22}N_2O_5S$: C, 58.44; H, 5.69; N, 7.18; S, 8.21. Found: C, 58.11; H, 5.65; N, 7.44; S, 8.41.

5.1.5.3. (±)*-2-Methoxyethyl 3-acetyl-4-(benzo[d][1,3]dioxol-5-yl)-6-methyl-2-thioxo-1,2,3,4-tetrahydropyrimidine-5-carboxylate* **(9c)**

Yield (0.30 g, 73 %) as yellow crystal with m.p. 147 -148 °C. ^{1}H NMR (400 MHz, DMSO-d_6) δ (ppm): 2.35 (3H, s, CH_3), 2.63 (3H, s, $COCH_3$), 3.24 (3H, s, OCH_3), 3.52-3.55 (2H, m, CH_2OCH_3), 4.16-4.21 (1H, m, $COOCH_2$), 4.25-4.30 (1H, m, $COOCH_2$), 6.00 (2H, s, OCH_2O), 6.33 (1H, s, pyrimidine 4-H), 6.70 (1H, dd, *J* = 8.0, 1.2 Hz, 6-H), 6.72 (1H, d, *J* = 1.2 Hz, 4-H), 6.87 (1H, d, *J* = 8.0 Hz, 7-H), 11.71 (1H, s, 1-NH). ^{13}C NMR (100 MHz, DMSO) δ (ppm): 16.92, 27.66, 53.03, 58.53, 63.76, 70.23, 101.66, 107.10, 107.59, 108.61, 120.05, 133.24, 145.61, 147.35, 147.91, 165.15, 173.57, 178.35. EI-MS: *m/z*: 392.28 [M^+]. Anal. Calcd. for $C_{18}H_{20}N_2O_6S$: C, 55.09; H, 5.15; N, 7.14; S, 8.17. Found: C, 55.19; H, 5.09; N, 7.35; S, 8.37.

5.1.5.4. (±)*-Benzyl 3-acetyl-4-(benzo[d][1,3]dioxol-5-yl)-6-methyl-2-thioxo-1,2,3,4-tetrahydro-pyrimidine-5-carboxylate* **(9d)**

Yield (0.26 g, 59%) as yellow crystal with m.p. 169-170 °C. ^{1}H NMR (400 MHz, DMSO-d_6) δ (ppm): 2.37 (3H, s, CH_3), 2.62 (3H, s, $COCH_3$), 5.15 (1H, d, *J* = 12.8 Hz, $COOCH_2$), 5.22 (1H, d, *J* = 12.8 Hz, $COOCH_2$), 6.00 (2H, s, OCH_2O), 6.39 (1H, s, pyrimidine 4-H), 6.67 (1H, d, *J* = 8.0 Hz, 6-H), 6.69 (1H, s, 4-H), 6.85 (1H, d, *J* = 8.0 Hz, 7-H), 7.28 – 7.35 (5H, m, Bn-H_5), 11.74 (1H, s, 1-NH). ^{13}C NMR (100 MHz, DMSO) δ (ppm): 16.97, 27.61, 52.91, 66.21, 101.70, 107.22, 107.31, 108.64, 120.32, 128.22, 128.48, 128.90, 133.03, 136.55, 145.99, 147.44, 147.94, 164.97, 173.49, 178.30. EI-MS: *m/z*: 424.18 [M^+]. Anal. Calcd. for $C_{22}H_{20}N_2O_5S$: C, 62.25; H, 4.76; N, 6.60; S, 7.56. Found: C, 62.40; H, 5.01; N, 6.79, S, 7.75.

5.1.6. General procedure for preparation of DHPM compounds **(10a–d, 11a–b,** *and* **12)**

A mixture of the corresponding β-diketones or dimedone (40 mmol), compound **4** (25 mmol), thiourea **7a** / urea **7b** (50 mmol), citric acid (25 mmol) and triethylorthoformate (50 mmol) was heated under reflux for 16 h. The reaction was quenched by addition of dist. water (15 ml) and the mixture was then cooled in an ice-bath. The precipitated solid was filtered, and recrystallized from DMF/Acetone to give the corresponding products **(10a–d, 11a–b,** and **12)**.

5.1.6.1. (±)*-5-Acetyl-4-(benzo[d][1,3]dioxol-5-yl)-6-methyl-3,4-dihydropyrimidin-2(1H)-thione* **(10a)**

Yield (0.17 g, 56%) as white powder with m.p. 250-251 °C, (Lit. m.p. 238-240 °C) [56]. ^{1}H NMR (400 MHz, DMSO-d_6) δ (ppm): 2.14 (3H, s, CH_3), 2.33 (3H, s, $COCH_3$), 5.21 (1H, s, pyrimidine 4-H), 6.00 (2H, s, OCH_2O), 6.69 (1H, d, *J* = 6.4 Hz, 6-H), 6.76 (1H, s, 4-H), 6.88 (1H, d, *J* = 6.4 Hz, 7-H), 9.73 (1H, s, 3-NH), 10.29 (1H, s, 1-NH). ^{13}C NMR (100 MHz, DMSO) δ (ppm): 18.69, 30.79, 53.97, 101.57, 107.45, 108.68, 110.74, 120.32, 137.32, 145.03, 147.22, 147,94, 174.31, 195.37. EI-MS: *m/z*: 290.03 [M^+]. Anal. Calcd. for $C_{14}H_{14}N_2O_3S$: C, 57.91; H, 4.87; N, 9.65; S, 11.05; Found: C, 57.85; H, 4.66; N, 9.42; S, 11.12.

5.1.6.2. (±)-*(4-(Benzo[d][1,3]dioxol-5-yl)-6-methyl-2-thioxo-1,2,3,4-tetrahydropyrimidin-5-yl) (phenyl) methanone* **(10b)**

Yield (0.25 g, 68 %) as yellow powder with m.p. 185-187 ^{o}C. ^{1}H NMR (400 MHz, DMSO-d_6: DMF mixture) δ (ppm): 1.73 (3H, s, CH_3), 5.21 (1H, s, pyrimidine 4-H), 6.00 (2H, s, OCH_2O), 6.64 (1H, d, *J* = 8.0 Hz, 6-H), 6.72 (1H, s, 4-H), 6.86 (1H, d, *J* = 8.0 Hz, 7-H), 7.44 – 7.56 (5H, m, C_6H_5CO), 9.65 (1H, s, 3-NH) , 10.36 (1H, s, 1-NH). ^{13}C NMR (100 MHz, DMSO: DMF mixture) δ (ppm): 18.39, 55.50, 101.57, 107.17, 108.69, 110.60, 120.18, 128.41, 129.16, 132.41, 137.44, 140.54, 142.19, 147.18, 147.91, 174.46, 194.99. EI-MS: m/z (%): 352.25 [M^+]. Anal. Calcd. for $C_{19}H_{16}N_2O_3S$: C, 64.75; H, 4.59; N, 7.95; S, 9.10. Found: C, 64.47; H, 4.78; N, 8.21; S, 9.40.

5.1.6.3. (±)-*5-Acetyl-4-(benzo[d][1,3]dioxol-5-yl)-6-methyl-3,4-dihydropyrimidin-2(1H)-one* **(10c)**

Yield (0.14 g, 49%) as faint brown powder with m.p. 260-262 ^{o}C, (Lit. m.p. 262 ^{o}C) [56]. ^{1}H NMR (400 MHz, DMSO-d_6) δ (ppm): 2.09 (3H, s, CH_3), 2.28 (3H, s, $COCH_3$), 5.18 (1H, s, pyrimidine 4-H), 5.99 (2H, s, OCH_2O), 6.70 (1H, d, *J* = 8.0 Hz, 6-H), 6.78 (1H, s, 4-H), 6.86 (1H, d, *J* = 8.0 Hz, 7-H), 7.78 (1H, s, 3-NH), 9.19 (1H, s, 1-NH). ^{13}C NMR (100 MHz, DMSO) δ (ppm): 19.34, 30.69, 54.02, 101.44, 107.39, 108.58, 109.85, 119.99, 138.70, 146.90, 147.84, 148,58, 152.50, 194.84. EI-MS: *m/z*: 273.97 [M^+]. Anal. Calcd. for $C_{14}H_{14}N_2O_4$: C, 61.31; H, 5.16; N, 10.22; Found: C, 61.13; H, 5.31; N, 10.36.

5.1.6.4. (±)-*(4-(Benzo[d][1,3]dioxol-5-yl)-6-methyl-2-oxo-1,2,3,4-tetrahydropyrimidin-5-yl) (phenyl) methanone* **(10d)**

Yield (0.15 g, 43 %) as yellow crystals with m.p. 214-215 ^{o}C. ^{1}H NMR (400 MHz, DMSO-d_6: DMF mixture) δ (ppm): 1.68 (3H, s, CH_3), 5.23 (1H, s, pyrimidine 4-H), 5.98 (2H, s, OCH_2O), 6.66 (1H, dd, *J* = 8.0, 1.4 Hz, 6-H), 6.74 (1H, d, *J* = 1.4 Hz, 4-H), 6.83 (1H, d, *J* = 8.0 Hz, 7-H), 7.42 – 7.54 (5H, m, C_6H_5CO), 7.77 (1H, s, 3-NH), 9.19 (1H, s, 1-NH). ^{13}C NMR (100 MHz, DMSO: DMF mixture) δ (ppm): 18.98, 55.41, 101.42, 107.11, 108.53, 109.84, 119.88, 128.22, 129.04, 131.92, 138.77, 141.45, 145.96, 146.83, 147.77, 152.56, 194.76. EI-MS: m/z (%): 336.24 [M^+]. Anal. Calcd. for $C_{19}H_{16}N_2O_4$: C, 67.85; H, 4.80; N, 8.33. Found: C, 67.56; H, 4.61; N, 8.11.

5.1.6.5. (±)-*4-(Benzo[d][1,3]dioxol-5-yl)-2-thioxo-1,2,3,4-tetrahydro-5H-indeno[1,2-d]-pyrimidin-5-one* **(11a)**

Yield (0.19 g, 54 %) as yellow crystals with m.p. 214-215 ^{o}C (Lit. m.p. 220-222 ^{o}C) [57]. ^{1}H NMR (400 MHz, DMSO-d_6) δ (ppm): 6.22 (2H, s, OCH_2O), 7.15 (1H, d, *J* = 8.0 Hz, 7-H), 7.79 (1H, s, pyrimidine 4-H), 7.93 – 8.01 (7H, m, indene 6,7,8,9-H_4 + 6-H + 1-NH + 3-NH), 8.54 (1H, d, *J* = 1.2 Hz, 4-H). ^{13}C NMR (100 MHz, DMSO) δ (ppm): 102.94, 109.29, 112.32, 123.35, 123.46, 127.06, 128.03, 133.62, 136.14, 136.26, 139.75, 142.24, 146.42, 148.22, 152.78, 189.52, 190.19. EI-MS: *m/z*: 336.87 [M^+]. Anal. Calcd. for $C_{18}H_{12}N_2O_3S$: C, 64.27; H, 3.60; N, 8.33; S, 9.53. Found: C, 64.35; H, 3.51; N, 8.23; S, 9.46.

5.1.6.6. (±)*-4-(Benzo[a][1,3]dioxol-5-yl)-3,4-dihydro-1H-indeno[1,2-a]pyrimidine-2,5-dione* **(11b)**

Yield (0.17 g, 51 %) as yellow crystals with m.p. 210-211 °C (Lit. m.p. 217-219 °C) [57]. ^{1}H NMR (400 MHz, DMSO-d_6) δ (ppm): 6.22 (2H, s, OCH_2O), 7.14 (1H, d, *J* = 8.0 Hz, 7-H), 7.78 (1H, s, pyrimidine 4-H), 7.93 – 8.01 (7H, m, indene 6,7,8,9-H_4 + 6-H + 1-NH + 3-NH), 8.53 (1H, d, *J* = 1.2 Hz, 4-H). ^{13}C NMR (100 MHz, DMSO) δ (ppm): 102.94, 109.30, 112.32, 123.36, 123.47, 127.06, 128.03, 133.63, 136.15, 136.27, 139.75, 142.24, 146.42, 148.23, 152.79, 189.53, 190.20. EI-MS: *m/z*: 319.98 [M^+]. Anal. Calcd. for $C_{18}H_{12}N_2O_4$: C, 67.50; H, 3.78; N, 8.75. Found: C, 67.75; H, 3.88; N, 8.94.

5.1.6.7. (±)*-4-(Benzo[d][1,3]dioxol-5-yl)-7,7-dimethyl-4,6,7,8-tetrahydroquinazoline-2,5(1H,3H)-dione* **(12)**

Yield (0.19 g, 58 %) as faint yellow powder with m.p. 178 -179 °C. ^{1}H NMR (400 MHz, DMSO-d_6) δ (ppm): 0.92 (3H, s, CH_3), 1.02 (3H, s, CH_3), 2.05 (1H, d, *J* = 16.0 Hz, quinazoline 6-H), 2.19 (1H, d, *J* = 16.0 Hz, quinazoline 6-H), 2.29 (1H, d, *J* = 17.2 Hz, quinazoline 8-H), 2.40 (1H, d, *J* = 17.2 Hz, quinazoline 8-H), 5.08 (1H, s, quinazoline 4-H), 5.98 (2H, s, OCH_2O), 6.70 (1H, dd, *J* = 8.0, 1.3 Hz, 6-H), 6.73 (1H, d, *J* = 1.3 Hz, 4-H), 6.85 (1H, d, *J* = 8.0 Hz, 7-H), 7.74 (1H, s, 3-NH) , 9.48 (1H, s, 1-NH). ^{13}C NMR (100 MHz, DMSO) δ (ppm): 27.42, 29.14, 32.77, 39.49, 50.27, 52.11, 101.37, 107.11, 107.85, 108.47, 119.79, 139.17, 146.68, 147.61, 152.32, 152.84, 193.44. EI-MS: *m/z*: 314.03 [M^+]. Anal. Calcd. for $C_{17}H_{18}N_2O_4$: C, 64.95; H, 5.78; N, 8.91. Found: C, 64.83; H, 5.52; N, 8.78.

5.1.7. General procedure for preparation of compounds **(15** *and* **16)**

A mixture of compound **4** (10 mmol), 2- aminobenzimidazole **14** (10 mmol) and acetyl acetone / benzyl acetoacetate (10 mmol) in DMF (30 ml) was heated under reflux for 10 hours. After cooling to room temperature, acetone (15 ml) was added. The reaction mixture was permitted to stand overnight and then filtered to yield precipitated solid of product, which was recrystallized from DMF/acetone.

5.1.7.1. (±)*-Benzyl4-(benzo[d][1,3]dioxol-5-yl)-2-methyl-1,4-dihydrobenzo[4,5]imidazo[1,2-a] pyrimidine -3-carboxylate* **(15)**

Yield (0.38 g, 83%) as white powder with m.p. 258-260 °C. ^{1}H NMR (400 MHz, DMSO-d_6) δ (ppm): 2.48 (3H, s, CH_3), 5.05 (1H, d, *J* = 12.8 Hz, $COOCH_2$), 5.16 (1H, d, *J* = 12.8 Hz, $COOCH_2$), 5.94 (2H, s, OCH_2O), 6.41 (1H, s, pyrimidine 4-H), 6.75 (1H, d, *J* = 8.0 Hz, 7-H), 6.84 (1H, d, *J* = 8.0 Hz, 6-H), 6.88 (1H, s, 4-H), 6.98 (1H, t, *J* = 7.2 Hz, benzimidazole 5-H), 7.05 (1H, t, *J* = 7.2 Hz, benzimidazole 6-H), 7.21 (2H, d, *J* = 7.2 Hz, benzimidazole 4,7-H_2), 7.31 – 7.36 (5H, m, Bn-H_5), 10.90 (1H, br s, 1-NH). ^{13}C NMR (100 MHz, DMSO) δ (ppm): 19.30, 56.03, 65.41, 98.00, 101.55, 108.08, 108.44, 110.65, 117.25, 120.67, 121.15, 122.24, 128.12, 128.19, 128.72, 131.94, 136.29, 136.96, 142.72, 145.85, 147.20, 147.68, 165.48. EI-MS: *m/z*: 439.20 [M^+]. Anal. Calcd. for

$C_{26}H_{21}N_3O_4$: C, 71.06; H, 4.83; N, 9.56; Found: C, 71.29; H, 4.67; N, 9.72.

5.1.7.2. (±)-*1-(4-(Benzo[d][1,3]dioxol-5-yl)-2-methyl-1,4-dihydrobenzo[4,5]imidazo[1,2-a] pyrimidin-3-yl)ethan-1-one* **(16)**

Yield (0.20 g, 55%) as white powder with m.p. 250-252 °C. ^{1}H NMR (400 MHz, DMSO-d_6) δ (ppm): 2.24 (3H, s, CH_3), 2.48 (3H, s, $COCH_3$), 5.93 (2H, s, OCH_2O), 6.54 (1H, s, pyrimidine 4-H), 6.80 (1H, d, *J* = 8.0 Hz, 6-H), 6.94 (1H, d, *J* = 8.0 Hz, 7-H), 6.95 (1H, s, 4-H), 7.02 (1H, t, *J* = 7.6 Hz, benzimidazole 5-H), 7.06 (1H, t, *J* = 7.6 Hz, benzimidazole 6-H), 7.35 (1H, d, *J* = 7.6 Hz, benzimidazole 4-H), 7.47 (1H, d, *J* = 7.6 Hz, benzimidazole 7-H), 10.80 (1H, s, 1-NH). ^{13}C NMR (100 MHz, DMSO) δ (ppm): 20.19, 31.11, 55.83, 101.58, 107.98, 108.53, 109.09, 110.67, 117.31, 120.65, 121.24, 122.27, 132.02, 136.02, 142.75, 145.89, 146,57, 147.26, 147.84, 194.78. EI-MS: *m/z*: 347.59 [M^+]. Anal. Calcd. for $C_{20}H_{17}N_3O_3$: C, 69.15; H, 4.94; N, 12.09; Found: C, 69.42; H, 5.21; N, 11.93.

5.2. Biology

5.2.1. Preliminary in vitro anticancer screening [58]

The human tumor cell lines of the cancer screening panel are grown in RPMI 1640 medium containing 5% fetal bovine serum and 2 mM L-glutamine. For a screening experiment, cells are injected into 96 well micro titer plates in 100 µl at plating densities ranging from 5,000 to 40,000 cells/well depending on the doubling time of separate cell lines. After cell inoculation, incubation of the micro titer plates was done at 37° C, 5 % CO2, 95 % air and 100 % relative humidity overnight prior to adding of experimental drugs. After 24 h, each cell line of two plates are fixed in situ with TCA, to represent a calculation of the cell population for each cell line at the time of drug addition. Experimental drugs are solubilized in DMSO at 400-fold the final maximum test concentration and kept frozen prior to use. At the time of drug addition, an aliquot of frozen concentrate is thawed and diluted to twice the wanted final maximum test concentration with complete medium containing 50 µg/ml gentamicin. Aliquots of 100 µl of these different dilutions of drug are added to the suitable microtiter wells previously containing 100 µl of medium, leading to the required final drug concentrations 10 µM. Controls, containing only DMSO and phosphate buffer saline at identical dilutions, were done in the same method. Following drug addition, the plates are incubated for an extra 48 h at 37°C, 5 % CO2, 95 % air, and 100 % relative humidity. For adherent cells, the assay is finished by the addition of cold TCA. Cells are fixed in situ by the mild addition of 50 µl of cold 50% (w/v) TCA (final concentration, 10 % TCA) and incubated for 60 minutes at 4°C.

The supernatant is removed, and the plates are washed several times with dist. water and air dried. Sulforhodamine B (SRB) solution (100 µl) at 0.4 % (w/v) in 1 % acetic acid is added to each well, and plates are incubated for ten minutes at 25°C.

After staining, unbound dye is discarded by washing several times with 1 % acetic acid and the plates are air dried. Bound stain is then solubilized with 10 mM trizma base, and the absorbance is recorded on an automated reader at a wavelength of 515 nm. For suspension cells, the methodology is the similar except that the assay is finished by fixing settled cells at the bottom of the wells by gradually adding 50 µl of 80 % TCA (final conc., 16 % TCA). Using the seven absorbance measurements, the percentage growth of the treated cells is calculated compared to the untreated control cells.

5.2.2. Kinesin inhibition assay

ATPase assays were performed as previously described [23, 59] by measuring the inhibition of basal ATPase activity of human $Eg5_{1–368}$ at an estimated protein concentration between 200 and 400 nm. The Eg5 concentration was estimated by the Bradford reagent. All data were measured in triplicate, and IC_{50} values are given as mean values ±SD. Detailed procedure for kinesin inhibition assay is available in supplementary information (SI).

5.2.3. HEK-293 cell growth inhibition assay

Detailed procedure for HEK 293 cell growth inhibition assay with representative IC_{50} curves were discussed in SI as previously described [60]. All data were measured in triplicate, and IC_{50} values are given as mean values ±SD.

5.2.4. Cell cycle analysis and induction of apoptosis

5.2.4.1. Flow cytometric analysis of cell-cycle distribution

Cell cycle analysis was carried out through flow cytometry [61]. SNB-75 cells were treated with the test compound, seeded and incubated for 24 hours at 37 °C, 5% CO_2. Cells were washed twice with phosphate buffer saline. Then, collection and centrifugation of cell pellets took place, followed by fixing with 70% (v/v) ethanol in ice for 15 minutes. Pellets were collected again, where they were incubated with propidium iodide (PI) staining solution that contains 50 µg/mL PI, 0.1 mg/mL RNAse A and 0.05% Triton X-100. After incubation for one hour at room temperature, it was analyzed by flow cytometry on FC500 cytometer (Beckman Coulter) and cell cycle distributions were calculated.

5.2.4.2. Analysis of cellular apoptosis

AnnexinV-fluorescein isothiocyanate (Annexin V-FITC) is a protein that possesses high affinity to phosphatidyl serine PS, which can be detected by staining with Annexin V- (FITC) and counter staining with propidium iodide (PI). Apoptosis was initially induced by incubation of cells in a density of 1.2-1.8 X 10^4 cells/well in complete growing medium (100 µ L) with addition of the tested compound (100 µ L) in 96-microwell plates for 24 h. Then, 1-5 X 10^5 cells were collected by centrifugation and resuspended in 500 µ L of binding buffer. Annexin V-FITC (5 µ L) along with PI (5 µ L) were added and incubated in the dark for 5 minutes at room temperature. Analysis of Annexin-V-FITC binding was performed using FACS caliber flow cytometer (BD Biosciences, San Jose. CA).

5.2.5. Enzyme-Linked Immunosorbent Assay (ELISA) of caspase-3 and caspase-9

5.2.5.1.The invitrogen caspase-3 (active) human ELISA assay

The number of 8-well strips needed for the assay was determined. The standard diluent buffer (100 µL) was added to the zero standard wells, while chromogen blank was left empty. The standards, controls and tested compound (100 µL) were then added, and incubated for 2 hours at room temperature. Wells were evacuated from liquids, and washed 4 times. Caspase-3 (active) detection antibody solution (100 µL) was added to each well except the chromogen blank(s), and incubated for 1 hour at room temperature. Again liquid was discarded from wells and washed 4 times. Anti-Rabbit IgG HRP working solution was then added to each well excluding the chromogen blank and incubated for half an hour at room temperature. Wells were washed 4 times. Stabilized Chromogen (100 µL) was added to each well, and incubated for half an hour at room temperature. Finally, stop solution (100 µL) was added to each well and the absorbance was read at 450 nm within 2 hours after addition. Curve fitting software was used to generate the standard curve; from which the concentrations for tested compound and controls were read.

5.2.5.2.DRG® caspase-9 (human) ELISA (EIA-4860) assay

First, cell lysates were prepared. The number of required microwell strips was determined and allowed to be washed twice with wash buffer. The sample diluent was added in duplicate to the blank wells (100 µL) and to sample wells (50 µL). The sample was added in duplicate (50 µL) to designated sample wells. Detection antibody (50 µL) was prepared and added to all wells, and incubated for 2 hours at room temperature. Microwell strips were washed 3 times with wash buffer. Anti-rabbit-IgG-HRP was prepared and added (100 µL) to all wells, then incubated for 1 hour at room temperature. Microwell strips were washed 3 times with wash buffer. TMB substrate solution (100 µL) was added, and incubated for 10 minutes at room temperature. Finally, stop solution (100 µL) was added, and the color intensity was measured at 450 nm.

5.3. Molecular modeling

The three-dimensional structure of kinesin was downloaded as a PDB file from the RCSB Protein Data Bank (PDB ID: 1Q0B). The PDB file of the protein was opened in UCSF Chimera version 1.13.1 and all non-standard atoms and bonds were removed. This protein was opened in AutoDock vina where the co-ordinates of the binding pocket were determined using the grid box function. The grid box size was set to 25.5446 × 27.2512 × 23.3912 points with a grid box center of 18.9547 × 15.8184 × 109.135. Using the dock prep function, water molecules were deleted, partial charges were assigned and hydrogens were added to the protein. The protein was then saved in the Mol 2 format ready for the docking stage. The synthesized dihydropyrimidine derivatives were drawn, optimized, and saved in a mol2 format with the aid of ChemDraw Professional 18.1 Suite. The canonical

SMILES of the compounds were entered into UCSF Chimera using the build structure tool. The compound was then ready by adding hydrogens using the "structure editing function" and moved the system towards energy minimization using the "minimize structure tool". The ligand was named and saved in the Mol2 format ready for the docking step. On a new UCSF Chimera session, firstly, the protein Mol2 file was opened followed by the target molecule. Using the surface/binding analysis tool, the AutoDock vina function was done. The protein PDB format was selected as the receptor and the target molecule SMILES was selected as the ligand. An output file was created and the binding pocket co-ordinates was entered. All ligand and receptor options were set as true and the exhaustiveness of search was set at the maximum of 8. Furthermore, the binding modes number was selected as 9. Vina.exe via a local path was selected as the executable location and docking was done.

References

[1] R.D. Vale, The Molecular Motor Toolbox for Intracellular Transport, Cell, 112 (2003) 467-480.

[2] A.J. Kim, S.A. Endow, A kinesin family tree, Journal of Cell Science, 113 (2000) 3681-3682.

[3] H. Epstein, J.M. Scholey, Kinesins in the spindle: an update, Trends Cell Biol., 2 (1992) 315-318.

[4] K.W. Wood, W.D. Cornwell, J.R. Jackson, Past and future of the mitotic spindle as an oncology target, Curr. Opin. Pharmacol., 1 (2001) 370-377.

[5] J.R. Jackson, D.R. Patrick, M.M. Dar, P.S. Huang, Targeted anti-mitotic therapies: can we improve on tubulin agents?, Nat. Rev. Cancer, 7 (2007) 107-117.

[6] S. Quasthoff, H.P. Hartung, Chemotherapy-induced peripheral neuropathy, Journal of Neurology, 249 (2002) 9-17.

[7] G. Bergnes, K. Brejc, L. Belmont, Mitotic kinesins: prospects for antimitotic drug discovery, Curr Top Med Chem, 5 (2005) 127-145.

[8] B. Nyamaa, H.K. Kim, Y.J. Jeong, I.-S. Song, J. Han, Kinesin Spindle Protein Inhibition in Translational Research, J Lipid Atheroscler, 3 (2014) 63-78.

[9] C. Perez-Melero, KSP inhibitors as antimitotic agents, Curr. Top. Med. Chem., 14 (2014) 2286-2311.

[10] E. Klein, S. DeBonis, B. Thiede, D.A. Skoufias, F. Kozielski, L. Lebeau, New chemical tools for investigating human mitotic kinesin Eg5, Bioorg. Med. Chem., 15 (2007) 6474-6488.

[11] A. Kamal, M.S. Malik, S. Bajee, S. Azeeza, S. Faazil, S. Ramakrishna, V. Naidu, M. Vishnuwardhan, Synthesis and biological evaluation of conformationally flexible as well as restricted dimers of monastrol and related dihydropyrimidones, Eur. J. Med. Chem., 46 (2011) 3274-3281.

[12] D.L. da Silva, F.S. Reis, D.R. Muniz, A.L.T. Ruiz, J.E. de Carvalho, A.A. Sabino, L.V. Modolo, Â. de Fátima, Free radical scavenging and antiproliferative properties of Biginelli adducts, Bioorg. Med. Chem., 20 (2012) 2645-2650.

[13] K.N. Venugopala, R. Govender, M.A. Khedr, R. Venugopala, B.E. Aldhubiab, S. Harsha, B. Odhav, Design, synthesis, and computational studies on dihydropyrimidine scaffolds as potential lipoxygenase inhibitors and cancer chemopreventive agents, Drug design, development and therapy, 9 (2015) 911.

[14] A.S. Mostafa, K.B. Selim, Synthesis and anticancer activity of new dihydropyrimidinone derivatives, Eur. J. Med. Chem., 156 (2018) 304-315.

[15] S. Kolb, O. Mondésert, M.L. Goddard, D. Jullien, B.O. Villoutreix, B. Ducommun, C. Garbay, E. Braud, Development of novel thiazolopyrimidines as CDC25B phosphatase inhibitors, ChemMedChem: Chemistry Enabling Drug Discovery, 4 (2009) 633-648.

[16] T.U. Mayer, T.M. Kapoor, S.J. Haggarty, R.W. King, S.L. Schreiber, T.J. Mitchison, Small

molecule inhibitor of mitotic spindle bipolarity identified in a phenotype-based screen, Science, 286 (1999) 971-974.

[17] I. Leizerman, R. Avunie-Masala, M. Elkabets, A. Fich, L. Gheber, Differential effects of monastrol in two human cell lines, Cell. Mol. Life Sci., 61 (2004) 2060-2070.

[18] Y. Zhang, W. Xu, Progress on kinesin spindle protein inhibitors as anti-cancer agents, Anticancer Agents Med. Chem., 8 (2008) 698-704.

[19] G. Cesare Tron, A. Minassi, G. Appendino, Pietro Biginelli: The man behind the reaction, Eur. J. Org. Chem., 2011 (2011) 5541-5550.

[20] L.H.S. Matos, F.T. Masson, L.A. Simeoni, M. Homem-de-Mello, Biological activity of dihydropyrimidinone (DHPM) derivatives: A systematic review, Eur. J. Med. Chem., 143 (2018) 1779-1789.

[21] P.J. Coleman, M.E. Fraley, Inhibitors of the mitotic kinesin spindle protein, Expert Opin. Ther. Pat., 14 (2004) 1659-1667.

[22] J.C. Cochran, S.P. Gilbert, ATPase mechanism of Eg5 in the absence of microtubules: Insight into microtubule activation and allosteric inhibition by monastrol, Biochemistry, 44 (2005) 16633-16648.

[23] H. Prokopcová, D. Dallinger, G. Uray, H.Y.K. Kaan, V. Ulaganathan, F. Kozielski, C. Laggner, C.O. Kappe, Structure activity relationships and molecular docking of novel dihydropyrimidine based mitotic Eg5 inhibitors, ChemMedChem, 5 (2010) 1760-1769.

[24] D. Russowsky, R.F.S. Canto, S.A.A. Sanches, M.G.M. D'Oca, Â. de Fátima, R.A. Pilli, L.K. Kohn, M.A. Antônio, J.E. de Carvalho, Synthesis and differential antiproliferative activity of Biginelli compounds against cancer cell lines: Monastrol, oxo-monastrol and oxygenated analogues, Bioorg. Chem., 34 (2006) 173-182.

[25] M.A. Bhat, A. Al-Dhfyan, M.A. Al-Omar, Targeting cancer stem cells with novel 4-(4-substituted phenyl)-5-(3, 4, 5-trimethoxy/3, 4-dimethoxy)-benzoyl-3, 4-dihydropyrimidine-2 (1H)-one/thiones, Molecules (Basel, Switzerland), 21 (2016) 1746-1755.

[26] I. Garcia-Saez, S. DeBonis, R. Lopez, F. Trucco, B. Rousseau, P. Thuéry, F. Kozielski, Structure of human Eg5 in complex with a new monastrol-based inhibitor bound in the R configuration, J. Biol. Chem., 282 (2007) 9740-9747.

[27] N. Razzaghi-Asl, M. Kamrani-Moghadam, B. Farhangi, R. Vahabpour, R. Zabihollahi, S. Sepehri, Design, synthesis and evaluation of cytotoxic, antimicrobial, and anti-HIV-1 activities of new 1,2,3,4-tetrahydropyrimidine derivatives, Res. Pharm. Sci., 14 (2019) 155-166.

[28] M. Gartner, N. Sunder-Plassmann, J. Seiler, M. Utz, I. Vernos, T. Surrey, A. Giannis, Development and biological evaluation of potent and specific inhibitors of mitotic kinesin Eg5, ChemBioChem, 6 (2005) 1173-1177.

[29] N. Kaur, K. Kaur, T. Raj, G. Kaur, A. Singh, T. Aree, S.-J. Park, T.-J. Kim, N. Singh, D.O. Jang, One-pot synthesis of tricyclic dihydropyrimidine derivatives and their biological evaluation, Tetrahedron, 71 (2015) 332-337.

[30] M.N. Aboul-Enein, A.A. El-Azzouny, M.I. Attia, Y.A. Maklad, K.M. Amin, M. Abdel-Rehim, M.F. El-Behairy, Design and synthesis of novel stiripentol analogues as potential anticonvulsants, Eur. J. Med. Chem., 47 (2012) 360-369.

[31] M.F. El-Behairy, T.E. Mazeed, A.A. El-Azzouny, M.N. Aboul-Enein, Design, synthesis and antibacterial potential of 5-(benzo[d][1,3]dioxol-5-yl)-3-tert-butyl-1-substituted-4,5-dihydropyrazoles, Saudi Pharm. J., 23 (2015) 202-209.

[32] F.H.S. Gama, R.O.M.A. de Souza, S.J. Garden, An efficient green protocol for the preparation of acetoacetamides and application of the methodology to a one-pot synthesis of Biginelli dihydropyrimidines. Expansion of dihydropyrimidine topological chemical space, RSC Adv., 5 (2015) 70915-70928.

[33] N. Daryabari, T. Akbarzadeh, M. Amini, R. Miri, H. Mirkhani, A. Shafiee, Synthesis and calcium channel antagonist activities of new derivatives of dialkyl 1,4-dihydro-2,6-dimethyl-4-(5-phenylisoxazol-3-yl)pyridine-3,5-dicarboxylates, J. Iran Chem. Soc., 4 (2007) 30-36.

[34] M. Khoshneviszadeh, N. Edraki, K. Javidnia, A. Alborzi, B. Pourabbas, J. Mardaneh, R. Miri, Synthesis and biological evaluation of some new 1,4-dihydropyridines containing different ester substitute and diethyl carbamoyl group as anti-tubercular agents, Bioorg. Med. Chem., 17 (2009) 1579-1586.

[35] R.F.S. Canto, A. Bernardi, A.M.O. Battastini, D. Russowsky, V.L. Eifler-Lima, Synthesis of dihydropyrimidin-2-one/thione library and cytotoxic activity against the human U138-MG and rat C6 glioma cell lines, J. Braz. Chem. Soc., 22 (2011) 1379-1388.

[36] A.M. Elmaghraby, I.A. Mousa, A.A. Harb, M.Y. Mahgoub, Three component reaction: An efficient synthesis and reactions of 3,4-dihydropyrimidin-2(1H)-ones and thiones using new natural catalyst, ISRN Org. Chem., 2013 (2013) 706437-706437.

[37] M. Kidwai, S. Saxena, M.K.R. Khan, S.S. Thukral, Synthesis of 4-aryl-7,7-dimethyl-1,2,3,4,5,6,7,8-octahydroquinazoline-2-one/thione-5-one derivatives and evaluation as antibacterials, Eur. J. Med. Chem., 40 (2005) 816-819.

[38] J. Valdez, R. Cedillo, A. Hernández-Campos, L. Yépez, F. Hernández-Luis, G. Navarrete-Vázquez, A. Tapia, R. Cortés, M. Hernández, R. Castillo, Synthesis and antiparasitic activity of ^{1}H-benzimidazole derivatives, Bioorg. Med. Chem. Lett., 12 (2002) 2221-2224.

[39] N.C. Institute, NCI-60 screening methodology, 2019.

[40] R. Ingle, S. Wadher, In-vitro cytotoxicity assay of quinoxalines, Curr. Pharm. Res., 6 (2015) 1751-1762.

[41] C.L. Rieder, A. Khodjakov, Mitosis Through the Microscope: Advances in Seeing Inside Live Dividing Cells, Science, 300 (2003) 91-96.

[42] T. Otto, P. Sicinski, Cell cycle proteins as promising targets in cancer therapy, Nat. Rev. Cancer, 17 (2017) 93-115.

[43] M. Andersson, J. Sjöstrand, A. Petersen, A.K.S. Honarvar, J. Karlsson, Caspase and proteasome activity during staurosporin-induced apoptosis in lens epithelial cells, Invest. Ophthalmol. Vis. Sci., 41 (2000) 2623-2632.

[44] K.M. Boatright, G.S. Salvesen, Mechanisms of caspase activation, Curr. Opin. Cell Biol., 15 (2003) 725-731.

[45] UCSF Chimera, 2019.

[46] N. Hirokawa, Y. Noda, Y. Tanaka, S. Niwa, Kinesin superfamily motor proteins and intracellular transport, Nat. Rev. Mol. Cell Biol., 10 (2009) 682-696.

[47] G. Woehlke, M. Schliwa, Walking on two heads: The many talents of kinesin, Nat. Rev. Mol. Cell Biol., 1 (2000) 50-58.

[48] Y. Yan, V. Sardana, B. Xu, C. Homnick, W. Halczenko, C.A. Buser, M. Schaber, G.D. Hartman, H.E. Huber, L.C. Kuo, Inhibition of a mitotic motor protein: Where, how, and conformational consequences, J. Mol. Biol., 335 (2004) 547-554.

[49] S.S. Rosenfeld, J. Xing, G.M. Jefferson, P.H. King, Docking and rolling, a model of how the mitotic motor Eg5 works, J. Biol. Chem., 280 (2005) 35684-35695.

[50] J.C. Cochran, J.E. Gatial, T.M. Kapoor, S.P. Gilbert, Monastrol inhibition of the mitotic kinesin Eg5, J. Biol. Chem., 280 (2005) 12658-12667.

[51] Z. Maliga, T.M. Kapoor, T.J. Mitchison, Evidence that monastrol is an allosteric inhibitor of the mitotic kinesin Eg5, Chem. Biol., 9 (2002) 989-996.

[52] A.S. Inc, Discovery studio Visualizer v19.1.0.18287 2019.

[53] H.B. El-Nassan, Advances in the discovery of kinesin spindle protein (Eg5) inhibitors as antitumor agents, Eur. J. Med. Chem., 62 (2013) 614-631.

[54] G.B. Dharma Rao, B.N. Acharya, M.P. Kaushik, An efficient synthesis of β-ketoesters via transesterification and its application in Biginelli reaction under solvent-free, catalyst-free conditions, Tetrahedron Lett., 54 (2013) 6644-6647.

[55] J. Xin, L. Chang, Z. Hou, D. Shang, X. Liu, X. Feng, An enantioselective Biginelli reaction catalyzed by a simple chiral secondary amine and achiral Brønsted acid by a dual-activation route, Chemistry–A European Journal, 14 (2008) 3177-3181.

[56] L.M. Ramos, B.C. Guido, C.C. Nobrega, J.R. Corrêa, R.G. Silva, H.C. de Oliveira, A.F. Gomes, F.C. Gozzo, B.A. Neto, The Biginelli reaction with an imidazolium–tagged recyclable iron catalyst: Kinetics, mechanism, and antitumoral activity, Chemistry–A European Journal, 19

(2013) 4156-4168.

[57] X. Wu, S.D. Kimball, P. Chen, D. Zhou, P. Shaoping, Compounds useful for treating disorders related to TRPA1, Google Patents, 2013.

[58] P. Skehan, R. Storeng, D. Scudiero, A. Monks, J. McMahon, D. Vistica, J.T. Warren, H. Bokesch, S. Kenney, M.R. Boyd, New colorimetric cytotoxicity assay for anticancer drug screening, J. Natl. Cancer Inst., 82 (1990) 1107-1112.

[59] S. DeBonis, J.P. Simorre, I. Crevel, L. Lebeau, D.A. Skoufias, A. Blangy, C. Ebel, P. Gans, R. Cross, D.D. Hackney, R.H. Wade, F. Kozielski, Interaction of the mitotic inhibitor monastrol with human kinesin Eg5, Biochemistry, 42 (2003) 338-349.

[60] T. Mosmann, Rapid colorimetric assay for cellular growth and survival: application to proliferation and cytotoxicity assays, Journal of immunological methods, 65 (1983) 55-63.

[61] T.M. Thornton, M. Rincon, Non-classical p38 map kinase functions: Cell cycle checkpoints and survival, Int. J. Biol. Sci., 5 (2008) 44-51.

Graphical Abstract

Design, synthesis, and bioactivity of dihydropyrimidine derivatives as kinesin spindle protein inhibitors

Haytham O. Tawfik, Mervat H. El-Hamamsy, Nabaweya A. Sharafeldin, and Tarek F. El-Moselhy

Compound **15** possessed potent activity against most cell lines in NCI (USA) protocol at the single concentration of 10 μM. It proved to have promising inhibitory influence against kinesin enzyme assay. Cell cycle analysis of SNB-75 cell treated with **15** showed cell cycle arrest at G2/M phase.

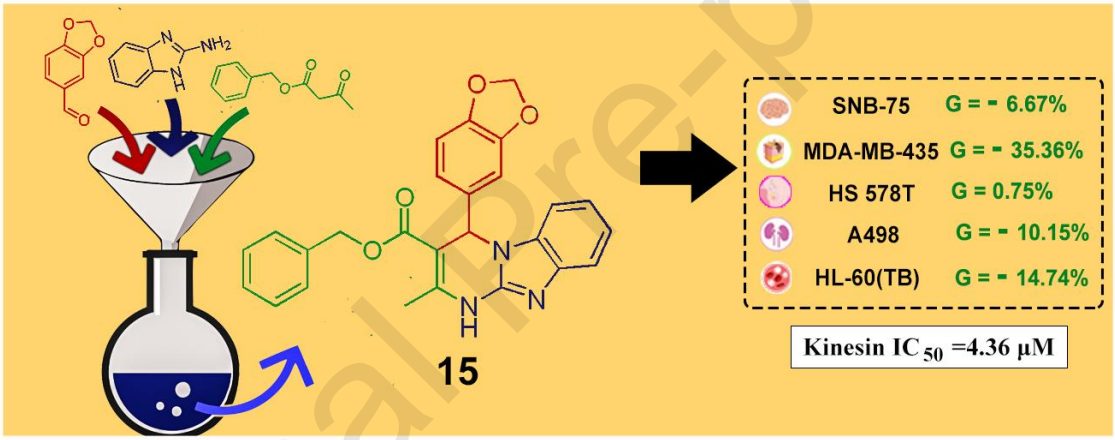

Highlights

- A novel series of dihydropyrimidine was designed and synthesized.
- Cytotoxic activity was assessed against 60 cancer cell lines.
- Compounds **10b** and **15** showed lethal activity mainly against MDA-MB-435 cell line.
- Compound **15** induced apoptosis and showed cell cycle arrest at G2/M phase.
- Compound **15** exhibited 4.5-fold increase in kinesin enzyme activity over monastrol.